GRADO EN INGENIERÍA EN TECNOLOGÍAS INDUSTRIALES

TRABAJO FIN DE GRADO

Design and Aerodynamic Analysis of a Formula Student Rear Wing

Author: Noelia María Prieto Sánchez

Supervisor: Raul de Lacerda

Madrid

September, 2023

Declaro, bajo mi responsabilidad, que el Proyecto presentado con el título

Design and Aerodynamic Analysis of a Formula Student Rear Wing

en la ETS de Ingeniería - ICAI de la Universidad Pontificia Comillas en el curso académico 20222-2023 es de mi autoría, original e inédito y no ha sido presentado con anterioridad a otros efectos. El Proyecto no es plagio de otro, ni total ni parcialmente y la información que ha sido tomada de otros documentos está debidamente referenciada.

Fdo.: Noelia María Prieto Sánchez Fecha: 31/ 08/ 2023

Autorizada la entrega del proyecto

EL DIRECTOR DEL PROYECTO

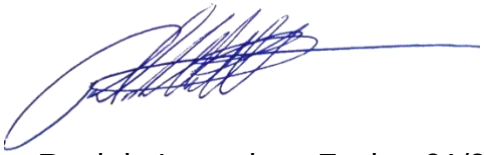

Fdo.: Raul de Lacerda Fecha: 01/09/2023

GRADO EN INGENIERÍA EN TECNOLOGÍAS INDUSTRIALES

TRABAJO FIN DE GRADO

Design and Aerodynamic Analysis of a Formula Student Rear Wing

Author: Noelia María Prieto Sánchez

Supervisor: Raul de Lacerda

Madrid

Septiembre de 2023

DISEÑO Y ANÁLISIS AERODINÁMICO DEL ALERÓN TRASERO DE UN FÓRMULA STUDENT

Autor: Prieto Sánchez, Noelia María.
Director: De Lacerda, Raul.
Entidad Colaboradora: ApeCS, Equipo de Formula Studen de CentraleSupélec

RESUMEN DEL PROYECTO

En este trabajo de Fin de Grado se lleva a cabo el diseño CAD mediante el programa SolidWorks del alerón trasero de un monoplaza de Formula Student y un estudio aerodinámico con el paquete CFD de ANSYS-FLUENT. Se analiza el resultado final con una propuesta de posibles futuras mejoras.

1. Introducción

La Formula Student es una competición internacional en la que estudiantes de ingeniería diseñan, construyen y compiten con autos de carreras tipo fórmula a escala real. Evalúa habilidades en diseño, rendimiento y gestión de proyectos, promoviendo el aprendizaje práctico y el trabajo en equipo entre los participantes de universidades de todo el mundo.

La importancia de la aerodinámica los alerones en competiciones como la Formula Student radica en su capacidad para generar carga aerodinámica, es decir fuerza en dirección hacia el suelo. Esto mejora la adherencia en el paso por curva y el rendimiento de los vehículos en la pista. Los alerones traseros son esenciales en el paquete aerodinámico de los monoplazas, desempeñando un papel fundamental. Estos componentes aerodinámicos han evolucionado desde su introducción en la década de 1960, optimizando la relación entre la carga aerodinámica y la resistencia al avance generadas.

En el presente trabajo de fin de grado se diseñará y analizará el alerón del primer monoplaza Formula Student del equipo ApeCS, de CentraleSupelec.

2. Objetivos

Con el objetivo general de construir un alerón trasero para el primer coche eléctrico ApeCS que participará en la Formula Student 2023, este Proyecto Fin de Carrera pretende alcanzar los siguientes objetivos:

1. Diseñar en formato CAD un alerón trasero que cumpla estrictamente con la normativa de competición.

2. El diseño del alerón debe minimizar la posterior dificultad y coste de construcción.

3. El alerón debe garantizar el mejor equilibrio entre las fuerzas de sustentación y resistencia.

Al tratarse del primer modelo diseñado por el equipo de ApecS, los objetivos son bastante sencillos. Se trata de diseñar un alerón que cumpla sus funciones básicas.

3. Metodología

Se diseñará un alerón de 2 elementos, un perfil aerodinámico principal y otro secundario o flap. Para cumplir con las restricciones dimensionales de Formula Student 2023, se diseñarán perfiles de 610mm de ancho y cuerda total de 450mm. Con el fin de seleccionar la mejor combinación de estos perfiles se lleva a cabo un estudio dividido en dos grandes etapas.

La primera, consistirá en la selección de los perfiles y ángulos de ataque más eficaces. Para ello, se elegirán 3 perfiles aerodinámicos conocidos en el estado del arte. Se diseñarán en dimensiones de perfil principal y flap con el programa *SolidWorks*. Por último, se evaluarán sus comportamientos a velocidad operacional para distintos ángulos de ataque. En base a estos resultados se seleccionarán los perfiles más adecuados para cada función (elemento principal y secundario).

En segundo lugar, se diseñarán distintas configuraciones que combinarán los perfiles de la selección anterior y diferentes distribuciones de cuerda (entre el 25%-30% de la cuerda total para el flap). Estas configuraciones serán analizadas nuevamente con el programa *ANSYS Fluent*. Se estudiarán los resultados obtenidos y se elegirá la configuración que mejor respecte los objetivos marcados.

4. Resultados

Etapa 1

En base a los objetivos, se eligieron 3 perfiles aerodinámicos a analizar:

- NACA 9517: Conocido por demostrar un equilibrio entre la carga aerodinámica generada y la resistencia.
- GOE 447: Elegido por ser la base de la experimentación en competiciones mayores como la Formula 1.
- E-423: Seleccionado por generar alta carga aerodinámica a bajas velocidades, característica que se alinea con los objetivos de la Formula Student.

Figura 1. Forma de los perfiles NACA 9517, GOE 447 y E 423. De izquierda a derecha.

Tras haber estudiado los coeficientes de sustentación y arrastre de cada perfil en función del ángulo de ataque, han destacado los resultados mostrados en la Tabla 1.

	Nombre	Ángulo de Ataque	F_L (N)	F_D (N)	F_L/F_D
Perfil Principal	GOE 447	5º	-20,1	2,55	-7,88
	NACA 9517	10º	-32,19	5,52	-5,83
Flap	NACA 9517	29º	-23,98	4,42	-5,43

Tabla 1. Resultados de la primera etapa.

Para el perfil principal se ha buscado elegir aquellos que generen menor resistencia, ya que esta será en su mayor parte producida por el flap. Por ello, en la elección de este elemento secundario se ha priorizado la generación de carga aerodinámica ya que todos generan alta resistencia por el elevado ángulo de ataque.

Etapa 2

La Tabla 2 muestra la numeración de las configuraciones diseñadas a partir de los perfiles seleccionados en la etapa anterior.

		Proporcion de la cuerda del flap					
Perfil Principal	**Perfil Flap**	25%	26%	27%	28%	29%	30%
GOE 447	NACA 9517	1.1	1.2	1.3	1.4	1.5	1.6
NACA 9517	NACA 9517	2.1	2.2	2.3	2.4	2.5	2.6

Tabla 2. Numeración de las combinaciones de perfiles y cuerdas.

En la siguiente figura se muestran los resultados de los análisis CFD de estas configuraciones.

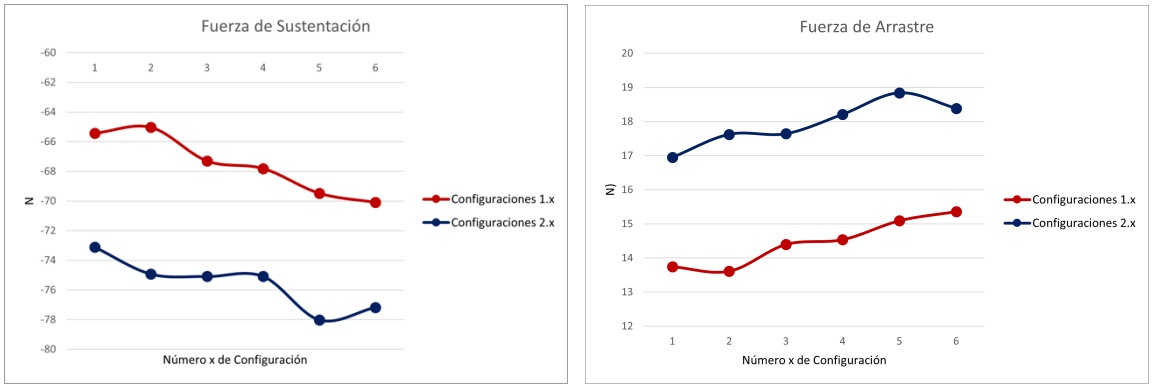

Figura 2: A la izquierda representación de la fuerza de sustentación generada por cada combinación. A la derecha representación de la fuerza de arrastre generada por cada combinación.

Los resultados de los análisis CFD muestran valores mayores de carga aerodinámica y resistencia para los perfiles de las configuraciones 2. Destaca el comportamiento de la configuración 2.3, ya que genera una fuerza de anti-sustentación similar a la de otras configuraciones con una resistencia inferior.

Por esta razón, y priorizando la generación de carga aerodinámica se elegirá configuración 2.3 como resultado final de este trabajo, con perfil principal NACA 9517 de cuerda 328,5mm y perfil secundario NACA 9517 de cuerda 121,5mm.

5. Conclusión

En el desarrollo de este proyecto, se han alcanzado los objetivos establecidos para el diseño de un aleron trasero para el coche de Formula Student del equipo ApeCS de CentraleSupélec.

El aleron final satisface las restricciones de dimensión impuestas por la competición. A lo largo del estudio, se ha asegurado que el ala cumpla su función principal generando carga aerodinámica para aumentar considerablemente el agarre sin descuidar la resistencia colateral. En lo que respecta al diseño, se ha buscado minimizar el costo de

construcción, reutilizando y reformando elementos ya fabricados y eligiendo perfiles con geometrías simples.
Si bien existen alerones más avanzados en otros equipos de Formula Student, gracias a la experiencia acumulada y a la oportunidad de iteración a lo largo de los años. En lo que respecta a este proyecto, el alerón diseñado representa un punto de partida importante y un paso fundamental en la buena dirección.

DESIGN AND AERODYNAMIC ANALYSIS OF A FORMULA STUDENT REAR WING

Author: Prieto Sánchez, Noelia María.
Director: De Lacerda, Raul.
Collaborating Entity: ApeCS, CentraleSupélec Formula Student Team

PROJECT SUMMARY

In this Final Degree Project, we will carry out the CAD design of the rear wing of a Formula Student single-seater and an aerodynamic study with the ANSYS-FLUENT CFD package and SolidWorks program. The final result is analyzed with a proposal for possible future improvements.

1. Introduction

Formula Student is an international competition in which engineering students design, build and race full-scale formula racing cars. It evaluates skills in design, performance and project management, promoting hands-on learning and teamwork among participants from universities around the world.

The importance of aerodynamic spoilers in competitions such as Formula Student lies in their ability to generate downforce, i.e. force in the direction of the ground. This improves cornering grip and vehicle performance on the track. Rear wings are essential to the aerodynamic package of single-seaters, playing a fundamental role. These aerodynamic components have evolved since their introduction in the 1960s, optimizing the relationship between downforce and drag generated.

In this thesis we will design and analyze the rear-wing of the first Formula Student single-seater of the ApeCS team, from CentraleSupelec.

2. Objectives

With the overall objective of building a rear wing for the first ApeCS electric car to participate in Formula Student 2023, this Final Year Project aims to achieve the following objectives:

1. Design in CAD format a rear wing that strictly complies with the competition regulations.

2. The design of the wing should minimize the subsequent difficulty and cost of construction.

3. The wing must ensure the best balance between lift and drag forces.

As this is the first model designed by the ApecS team, the objectives are quite simple. The aim is to design a rear wing that fulfills its basic functions.

3. Methodology

A 2-element wing will be designed, a main airfoil and a secondary airfoil or flap. To comply with the dimensional restrictions of Formula Student 2023, the profiles will be designed with a width of 610mm and a total chord of 450mm. In order to select the best combination of these airfoils, a study divided into two main stages will be carried out.

The first stage will consist of the selection of the most efficient profiles and angles of attack. For this purpose, 3 aerodynamic airfoils known in the state of the art will be chosen. They will be designed in main airfoil and flap dimensions with SolidWorks software. Finally, their behavior at operational speed will be evaluated for different angles of attack. Based on these results, the most suitable airfoils for each function (main and secondary element) will be selected.

The second step is to design different configurations combining the profiles of the previous selection and different chord distributions (between 25%-30% of the total chord for the flap). These configurations will be analyzed again with the ANSYS Fluent program. The results obtained will be studied and the configuration that best meets the objectives set will be chosen.

4. Results

Stage 1

Based on the objectives, 3 airfoils were chosen for analysis:

- NACA 9517: Known for demonstrating a balance between aerodynamic load generated and drag.
- GOE 447: Chosen for being the basis for experimentation in major competitions such as Formula 1.
- E-423: Selected for generating high downforce at low speeds, a feature that aligns with the objectives of Formula Student.

Figure 1. NACA 9517, GOE 447 and E 423 profiles. From left to right.

After studying the lift and drag coefficients of each airfoil as a function of the angle of attack, the most outstanding results are shown in Table 1.

	Name	Angle of attack	F_L (N)	F_D (N)	F_L/F_D
Main Profile	GOE 447	5º	-20,1	2,55	-7,88
	NACA 9517	10º	-32,19	5,52	-5,83
Flap	NACA 9517	29º	-23,98	4,42	-5,43

Table 1. Results from the first stage.

For the main airfoil, it has been sought to choose those that generate less drag, since most of it will be produced by the flap. Therefore, in the choice of this secondary element, priority has been given to the generation of aerodynamic load, since all of them generate high drag due to the high angle of attack.

Stage 2

Table 2 shows the numbering of the configurations designed from the profiles selected in the previous stage.

		Proportion of the flap's cord					
Main Profile	**Flap Profile**	25%	26%	27%	28%	29%	30%
GOE 447	NACA 9517	1.1	1.2	1.3	1.4	1.5	1.6
NACA 9517	NACA 9517	2.1	2.2	2.3	2.4	2.5	2.6

Table 2. Numbering of the profile and chord combinations.

The following figure shows the results of the CFD analysis of these configurations.

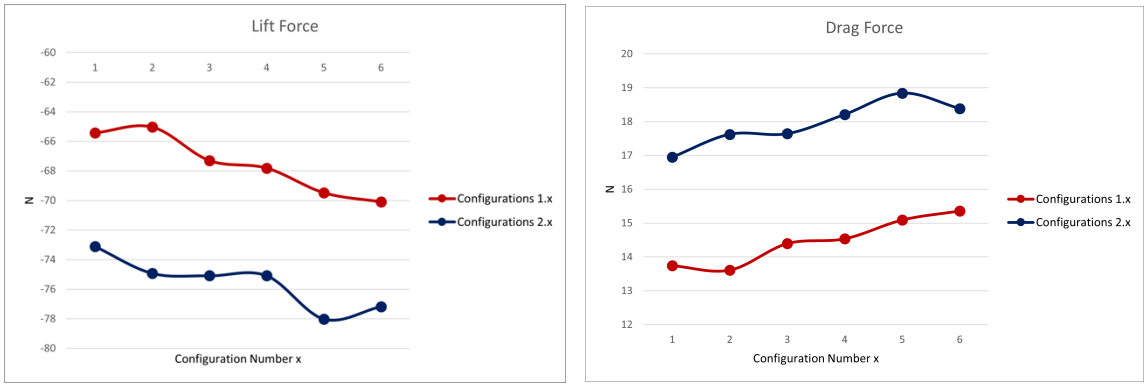

Figure 2: On the left, a representation of the lift force generated by each combination. On the right, a representation of the drag force generated by each combination.

The results of the CFD analysis show higher values of aerodynamic load and drag for the airfoils of configuration 2. The behavior of configuration 2.3 stands out, since it generates an anti-substantiation force similar to that of other configurations with a lower drag. It will be configuration 2.3, with main profile NACA 9517 chord 328.5mm and secondary profile NACA 9517 chord 121.5mm.

This result is taken prioritizing the main function of the aileron, the generation of downforce.

5. Conclusion

In the development of this project, the objectives set for the design of a rear wing for CentraleSupelec's Formula Student car have been achieved.

The final wing satisfies the dimensional constraints imposed by the competition. During the study, we made sure that the wing fulfills its main function by generating downforce to considerably increase grip without neglecting collateral drag. In terms of design, we have sought to minimize the cost of construction, reusing and reshaping elements already manufactured, and choosing profiles with simple geometries.

Although there are more advanced ailerons in other Formula Student teams, thanks to the accumulated experience and the opportunity for iteration over the years. As far as this project is concerned, the designed spoiler represents a starting point and a fundamental step in the right direction.

Contents

List of Figures

List of Tables

1 Introduction

Aerodynamics plays an essential role in motorsport. Its main function is to generate force towards the ground. This creates a "grip" effect on the track, called downforce. This action increases cornering speed, as there is more tyre surface in contact with the ground, the car does not skip and the driver has more control over the steering.

However, the elements designed for this purpose increase the aerodynamic drag of the car. Therefore, the main challenge of aerodynamics is to achieve an optimal balance between these two effects.

There are many elements that contribute to the aerodynamics of a racing car. One of the best known and most important are the spoilers.

In this Final Degree Project a rear wing of a formula car that will participate in the Formula Student competition will be designed and analysed.

1.1 Formula Student

Formula Student is the largest competition for university engineering students. Teams from universities around the world design and build a race car to compete in.

It was founded by the Society of Automotive Engineers in 1981, and the first competition in Europe took place in 1998. Today, several competitions are held each year in different countries around the world during the summer holidays, where teams can enter combustion, electric or even driver less single-seaters.

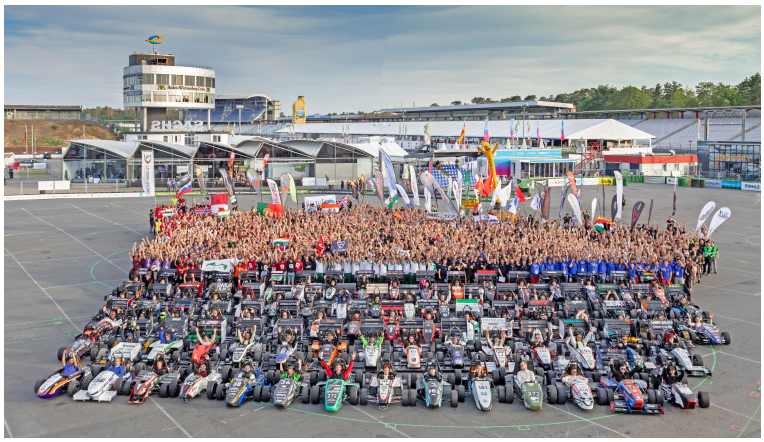

Figure 1: Participants of Formula Student Germany 2019 [Sie].

1.1.1 Emergence of ApeCS

France is not very well represented in this competition, as few teams from French universities participate in Formula Student. As students of one of the most prestigious French engineering schools and as passionate about the world of motorsport, we could not help but form a team to represent CentraleSupélec and France in Formula Student. Thus ApeCS, the CentraleSupélec Formula Student team, was born in September 2022. ApeCS will design and build an electric single-seater to participate in Formula Student in the summer of 2023.

Figure 2: Logo of CentraleSupélec's Formula Student team, ApeCS.

This Final Degree Project will present the design and aerodynamic analysis of the rear wing of this first single-seater of the ApeCS team that will compete in Formula Student.

1.1.2 Tests During the Competition

The Formula Student, unlike other competitions of this type, values other characteristics in addition to speed and for this reason different types of tests are established in this competition. Thus, we can find that the trials are divided into two types: static and dynamic. In addition to a previous technical inspection that does not contribute to the score of the competition but is required to participate in the events [FSG22].

Figure 3: Participating car being prepared for a technical test [dBC19].

Static Tests

These are made up of three major events:

- Bussines Plan Presentation: The objective of the BBP is to assess the team's ability to develop and deliver a complete business model, which must relate to the team's specific prototype race car entered in the competition. It should be presented to the jury as if it were a potential investor.
- Cost and Manufacturing Event: the objective of this second static test is to assess the team's knowledge of the manufacturing processes and costs associated with the construction of a prototype racing car. The team will be required to present the trade-off decisions made between content and cost.
- Engineering Design Event: For this event the team submits a report evaluating the student's engineering process and effort in designing a vehicle. In addition, the ability of the vehicle to drive autonomously will also be evaluated in this test.

Dynamic Tests

This comprises a total of 4 tests.

- Skipad Event: In this test the stability and cornering of the car is evaluated. The single-seater with its driver must drive around an 8-shaped circuit in the shortest

possible time.

- Acceleration Event: This test evaluates the vehicle's acceleration capacity in the natural conditions of the track, timing the time it takes the car to cover 75 meters accelerating from a standstill.

- Autocross Event: In this test, the car's cornering ability will be re-evaluated, as well as its acceleration and braking capacity. To do so, the car will have to drive a circuit of less than 1.5km.

- Endurance and efficiency Event: This test, dedicated to combustion single-seaters, will assess the mechanical endurance of the car and its ability to adapt from one driver to another. To this end, the vehicle will have to cover a total of 22 km on a circuit with a driver change at the halfway point. At the end, the amount of fuel used will be measured.

1.1.3 Rules on the Rear Wing

All single-seater regulations to be submitted by the teams can be found at [Stu23]. The following are the restrictions that will affect the design of the rear wing:

- Height: All aerodynamic devices behind the driver's seat set to its most rearward position must be lower than 1.2 m from the ground.

- Width: All aerodynamic devices higher than 500 mm from the ground, must not extend outboard of the most inboard point of the rear wheel/tire.

- Length: All aerodynamic devices must not extend further rearward than 250 mm from the rearmost part of the rear tires.

In addition, horizontal edges that may come into contact with any person shall have a minimum radius of 5 mm and vertical edges shall have a minimum radius of 3 mm.

This will affect the shape of the trailing edge of the aerofoils.

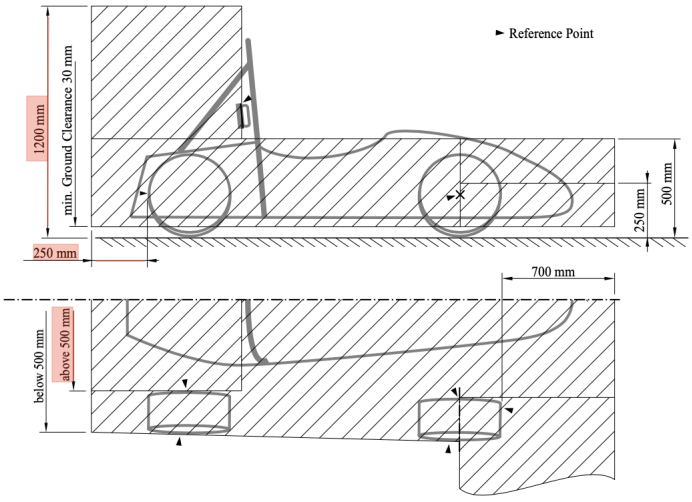

Figure 4: Restrictions on the dimensions of aerodynamic elements. Those affecting the rear wing are highlighted in red [Stu23].

2 State of the Question

2.1 Aerodynamics and Rear Spoiler Evolution

The desire to build fast and efficient vehicles has always been a human ambition. However, it was not until the middle of the last century that the focus turned to the development of aerodynamics. Until then, racing was based on designing high-performance engines that would make vehicles achieve a high top speed, and aerodynamics was inspired by elements of nature. Edmund Rumpler, a German inventor, built a car in the shape of a water droplet to reduce friction with the air [Lud70].

Figure 5: "Drop car" designed by Edmund Rumpler [Bla22].

The commercial automobile industry was not primarily concerned with the development of aerodynamic models. However, sports racing encouraged improvement and implemented aerodynamics in its designs. Thus, the greatest advances in aerodynamics occurred in the motorsport world from the 1960s onwards.

The first rear wing was designed by Chaparral, an American manufacturer of racing cars. Their Chaparral 2C car had an adjustable rear wing, which could be deployed to increase cornering grip and retracted to improve straight-line speed.

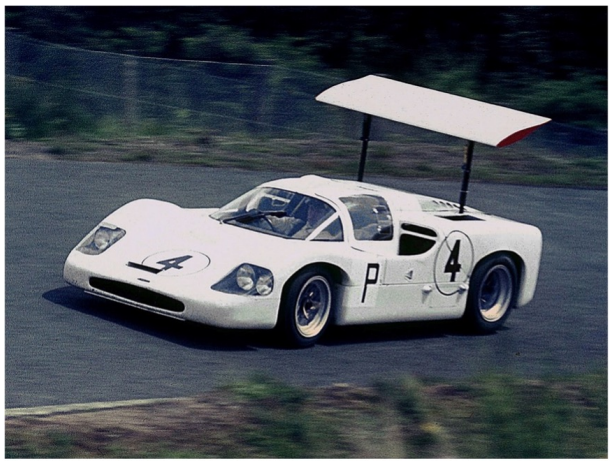

Figure 6: Chaparral 2F, one of the first cars to have a rear spoiler [Wikb].

In Formula 1, the first front wing was introduced in 1968 [F1]. The driving force was Colin Champman, who placed small raised spoilers on the nose of the Lotus 49B. This opened up a whole new field of research and gave way to the race for aerodynamic development.

Figure 7: Lotus 49B, the first Formula 1 model to incorporate spoilers [TIM21].

From then on, teams began to fit spoilers of different shapes and sizes on different areas of the car to test their effectiveness. It was common to place them high up, well away from the car, to take advantage of the clean air. However, the structures to which they were attached could not withstand the force they were subjected to. This, together with the fact that the wake left by the cars behind them was very turbulent, led to numerous accidents. Moreover, the lack of sophisticated wind tunnels and suitable tools at the time explains the failure of some of these inventions. As a result, spoilers were banned for a time.

Over time, teams succeeded in developing smaller spoilers closer to the surface of the car, and eventually spoilers became acceptable again under a series of regulations, which limited the dimensions, position, and methods of attachment to the rest of the car.

From the 1980s onwards, research began into a way of keeping the aerodynamic elements in the optimum position at all times. The first breakthrough in this area was active suspension, which fulfilled this objective. However, during the era of Formula 1's expansion as a show car, safety measures were tightened and in order to reduce cornering speeds, the use of active suspension was banned.

Since the 2000s, with the downsizing of engines, aerodynamics have become even more important. One of the latest developments, which is still in use today, is the implementation of DRS. This system consists of opening the rear wing to reduce the aerodynamic drag it generates in order to increase speed.

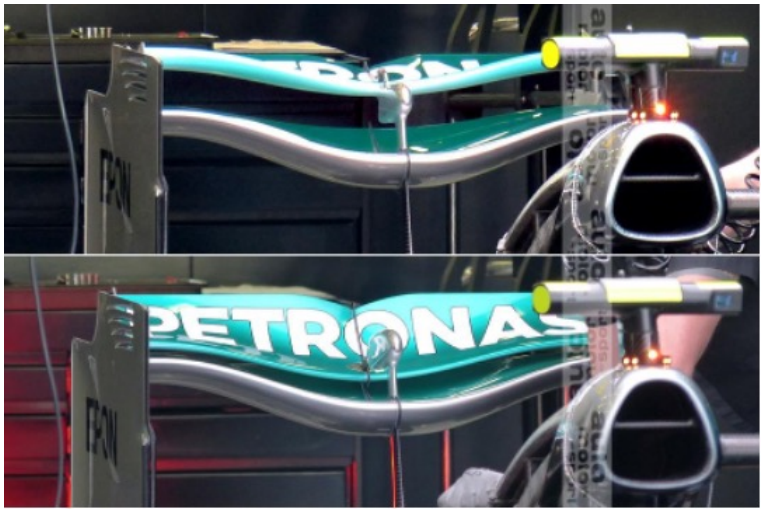

Figure 8: Rear wing DRS system. In the picture above it is open, in the picture below it is closed [Rod17].

2.2 Rear Wing Structure

Despite the constant evolution and changes to rear wings in major competitions such as Formula 1, they all maintain a constant two-part structure:

- Aerofoils: these are the fundamental elements of the wing. They are responsible for generating downforce thanks to their airfoil shape. They have the same geometry as an aircraft wing, but are placed in reverse in order to generate the opposite force.

- Endplates: These are the pieces that are placed at the lateral ends of the wing. These have two main functions. They prevent vortices (air movements from the upper surface to the lower surface), thus reducing induced drag. Their second function is to join the spoiler to the rest of the vehicle bodywork.

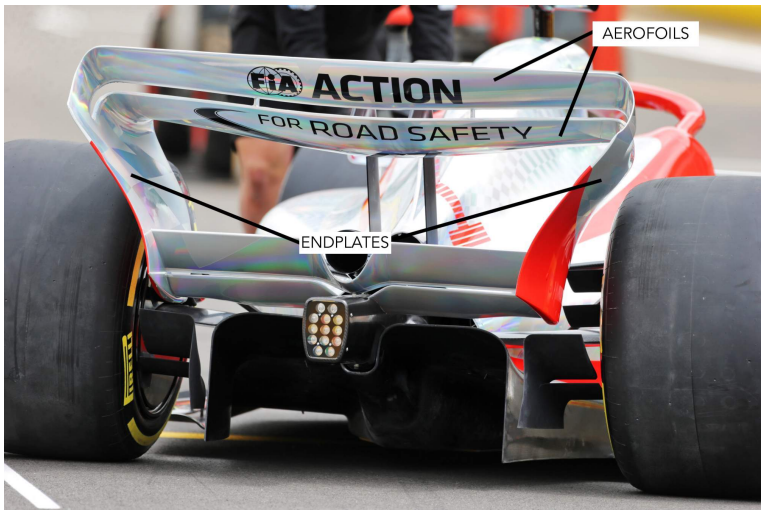

Figure 9: Rear of a Formula 1 single-seater.

2.3 Types of Spoiler

Although they have a well-defined structure, ailerons can be of different types depending on the number of winglets they contain.

2.3.1 Single-Element Spoilers

This is the most similar to the primitive aileron. It consists of a unique airfoil that generates all the downforce. The efficiency of this type of wing is limited to the design of the geometry of the single airfoil. Thus, in order to increase downforce, the curvature and thickness of the wing would have to be varied. winglets they contain.

2.3.2 Two-Element or Multi-Element Spoilers

This type of wing enhances the downforce generated by the single wing. The second airfoil, known as the flap, is positioned just behind and above the main one. This allows the boundary layer shedding of the main airfoil to be reduced and more downforce to be generated. This leads to an increase in drag [Gra].

There are two different geometries for this type of wing: A simpler one, the External Flap, which consists of the main airfoil and the flap. And a slightly more complex one, the Flap Fowler, which has a slot in the main airfoil. This allows for increased downforce at low speed.

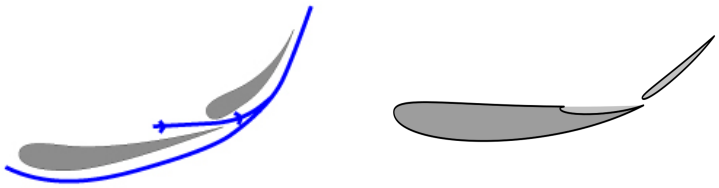

(a) External Flap (b) Fowler Flap

Figure 10: Possible geometries of a two-element spoiler [F1T13] [Wika].

Regarding the position of the two ailerons, experiments have determined that in order to prevent the wake of the main airfoil from interfering with the boundary layer of the flap, optimising the negative lift force, the following dimensions will be used [McB15]:

Parameter	Value
Gap	3,5%c
Overlap	5,2%c

Table 1: Space values between the main element and the flap of an aileron.

Gap is the distance between the two on the vertical axis, Overlap is the horizontal perposition distance and c is the value of the total chord. That is, the sum of the chords of both aerofoils.

As many flaps can be added as desired, this will still increase the downforce coefficient. However, the limit is at the time when drag increases noticeably with respect to downforce.

For two-element ailerons the most efficient total chord distribution is usually between 25% and 30% of the total chord for the flap.

3 Objectives

With the overall aim of building a rear wing for the first ApeCS electric car that will participate in Formula Student 2023, this Final Degree Project aims to achieve the following objectives:

1. To design in CAD format a rear wing that strictly complies with the competition regulations, set out in previous sections.

2. The design of the aileron should minimise the subsequent difficulty and cost of construction.

3. Perform a CFD analysis of the wing, which should ensure the best balance between lift and drag forces.

As this is the first model to be designed by the ApecS team, the objectives are rather straightforward. It is required to design an aileron that fulfils its basic functions.

4 Theoretical Underpinnings

In order to aerodynamically analyse the rear wing to be designed in this Final Degree Project, we will study its behaviour when it comes into contact with the air at operational speed. To do so, we will use fluid mechanics, the basic principles of which will be presented in this chapter [Dom23].

4.1 Fluids and their basic Properties

A fluid is a matter that changes shape continuously when subjected to shear stress. This is due to the low molecular cohesion of the particles which form it.

Within fluids we can differentiate between gases and liquids according to their compressibility.

A fluid can be considered as a continuous medium, which will allow us to replace the real matter of a discrete nature with a fictitious matter with the average properties of the real matter at that point.

In this Final Degree Project, the fluid to be taken into account will be air.

4.1.1 Density

It is defined as mass per amount of volume. Its units in the international system are kg/m^3.

$$\rho = \frac{m}{v} \tag{1}$$

For compressible fluids (gases) density depends on pressure and temperature, however for incompressible fluids (such as liquids) its density depends only on temperature. In this Final Degree Project we will consider air as an ideal gas, therefore its density will be governed by the following:

$$\rho = \frac{P}{RT} \tag{2}$$

Where:

- P is the pressure of the air (Pa).
- R is the Ideal Gas constant. In this case: 286,9 $\frac{J}{kgK}$.

- T is the air temperature (K)

4.1.2 Pressure

Pressure is the absolute value of the force per unit area; it is a scalar quantity.Its unit in the international system is the Pascal ($1Pa = 1N/m^2$). However, it is also common to work with other units such as bars ($1bar = 10^5 Pa$) or atmospheres ($1atm = 1.01396bar$).

It is possible to work with absolute or relative pressures, the difference between the two is the atmospheric pressure.

$$p_{atm} = p_{abs} - p_{rel} \tag{3}$$

4.1.3 Viscosity

Viscosity is defined as the fluid's resistance to movement; it can be compared to the friction in the movement of solids.

This parameter is found in all fluids, to a greater or lesser extent. It depends to a larger degree on the temperature of the fluid, and is greater in liquids than in gases. When talking about an ideal fluid, the effect of viscosity is very small and is not taken into account.

The dynamic viscosity μ gives the speed of deformation of a fluid under shear stress. Its units in the international system are $\frac{kg}{ms}$.

No-Slip Condition

The no-slip condition is a characteristic of viscous fluids. This characteristic implies that when the fluid comes into contact with a solid, the layer closest to the solid has a velocity of 0.

This phenomenon leads to the appearance of the so-called boundary layer, which will be described later.

4.1.4 Volumetric Modulus of Elasticity or Compressibility

Like solids, fluids exhibit compressive strength. This is not to be confused with their

non-resistance to shear stress, as mentioned above. The volumetric modulus of elasticity is the ratio between the pressure produced by external forces acting on the body surface and the volumetric deformation which is equal to the change in volume divided by the initial volume, while the temperature remains constant.

$$B = -V\left(\frac{\partial P}{\partial V}\right)_T = \rho\left(\frac{\partial P}{\partial \rho}\right)_T \tag{4}$$

Its unit is the Pascal (Pa).

4.1.5 Newtonian Fluid

Newtonian fluids are those whose motion is proportional to the force exerted on them. Thus, in Newtonian fluids, the frictional forces that appear between the layers of fluid in motion, for a contact surface dS, are given by Newton's formula:

$$\tau = \frac{-dF_{ROZ}}{dS} = \mu\frac{\partial v}{dn} \tag{5}$$

Where:

- τ is the shear stress,
- v is the flow velocity,
- n is the direction perpendicular to the flow stream.

Air is a Newtonian fluid.

4.2 Fluids Dynamics

Before presenting the basic equations of fluid dynamics, the different types of flow that can be encountered will be introduced.

Stationary/Non-Stationary Flow

Flow is said to be stationary if properties such as the velocity v(r) and density ρ(r) of the flow at one point do not depend on time, and non-stationary otherwise. This does

not mean that these properties must be the same at two different points, but only that at the same point they must not vary with time.

Compressible/Incompressible Flow

The flow is said to be compressible if the density ρ in it varies, as for example occurs in gases in the general case, while the flow is said to be incompressible when the density ρ hardly varies, as in the case for liquids.

Laminar or Turbulent Regime

Depending on the relative importance of viscous forces and inertial forces, the regime of motion of a fluid can be of two types:

- Laminar regime: The flow regime is said to be laminar when it has an orderly motion, in which the fluid particles move in parallel lines, with no mixing of matter between the different layers.
- Turbulent regime: The regime of motion of a fluid is turbulent when the fluid has a disorderly motion with intensive mixing between the different layers.

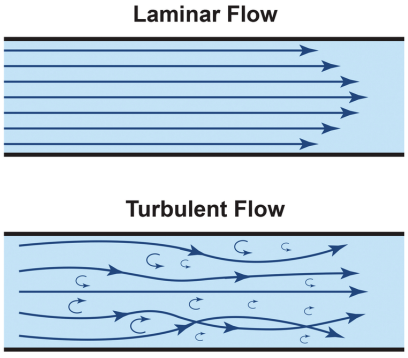

Figure 11: Graphical representation of the difference in motion in the layers of laminar and turbulent flow [Res].

Depending on the type of flow, laminar or turbulent, the frictional forces that appear will be of different types. In the case of laminar flow, the forces exerted between the different layers of the fluid are tangent to the direction of movement. On the other hand,

in the turbulent regime, a second contribution to the frictional force appears due to the mixing between the different layers.

The Reynolds number is used to determine the flow regime.

$$Re = \frac{\rho v L}{\mu} \tag{6}$$

L is the characteristic length of the fluid and v its velocity. The following table shows the limit values of the Reynolds number from which the flow is laminar or turbulent.

	Laminar Flow	Transitional Regime	Turbulent Flow
Internal Flow	$Re \leqslant 2300$	$2300 < Re < 4000$	$4000 \leqslant Re$
External Flow	$Re \leqslant 5 \times 10^5$		$5 \times 10^5 < Re$

Table 2: Scheme of transition from one regime to another according to Reynolds number.

4.2.1 Basic Equations of Fluid Mechanics

In the study of fluid motion, there are two classical methods. On the one hand, the Lagrangian method analyses the movement of each fluid particle as a function of time. This requires a large number of equations and is therefore often not useful. Euler's method, on the other hand, characterises the motion of the fluid by the density and velocity of the particles as a function of space and time. That is, we study a point in space, which we call the control volume (CV), and how the fluid moves at that point.

In most CFD (Computational Fluid Dynamics) software, the Eulerian approach is used.

Volumetric and Mass Flow Rate

In fluid mechanics we distinguish between two types of flow when studying its movement in a control volume:

- The volumetric flow rate : it consists of the volume of fluid that is displaced per unit of time. Its value can be determined with the following equation.

$$Q = \iint (\vec{v} \times \vec{n})\, dA = \vec{v} \times A \tag{7}$$

Its unit is $[m^3/s]$

- The mass flow rate : is the measure of mass passing through a surface per unit of time. It is calculated with the following equation.

$$\dot{m} = \iint \rho \left(\vec{v} \times \vec{n}\right) dA \tag{8}$$

Its unit is $[kg/s]$

4.2.2 Reynolds Transport Theorem

Before presenting the four fundamental rules, the conservation laws, that occur in a Control Volume the Reynolds Transport Theorem must be understood.

The Reynolds Transport Theorem relates the variation of the fluid to changes in the control volume as a function of time.

$$\frac{dB}{dt} = \frac{d}{dt} \iiint_{CV} \beta \rho dV + \iint_{CS} \beta \rho (\vec{v} \times \vec{n}) dA \tag{9}$$

Where,

- $\beta = \frac{dB}{dm}$
- B is the property of the fluid to be studied.
- CS is the control surface.
- CV is the control volume.

For a fixed control volume:

$$\frac{d}{dt} \iiint_{CV} \beta \rho dV = 0 \tag{10}$$

And

$$\frac{dB}{dt} = \iint_{CS} \beta \rho (\vec{v} \times \vec{n}) dA \tag{11}$$

4.2.3 Bernoulli's Equation or Principle

This principle describes the behaviour of a fluid moving along a streamline. Before stating it, it is necessary to know the following conservation theorems, which are derived from the Reynolds transport theorem for different B properties.

- Mass Conservation Equation:

$$\frac{dm}{dt} = \frac{d}{dt}\iiint_{CV} \rho dV + \iint_{CS} \rho(\vec{v} \times \vec{n}) dA = 0 \tag{12}$$

- Momentum Conservation Equation:

$$\frac{dm\vec{v}}{dt} = \frac{d}{dt}\iiint_{CV} \rho\vec{v} dV + \iint_{CS} \rho\vec{v}(\vec{v} \times \vec{n}) dA = \sum \vec{F} \tag{13}$$

- Angular Momentum Conservation Equation:

$$\frac{d(\vec{r} \times m\vec{v})}{dt} = \frac{d}{dt}\iiint_{CV} \rho(\vec{r} \times \vec{v}) dV + \iint_{CS} \rho(\vec{r} \times \vec{v})(\vec{v} \times \vec{n}) dA = \sum \vec{M} \tag{14}$$

- Energy Conservation Equation:

$$\frac{dQ}{dt} - \frac{dW}{dt} = \frac{dE}{dt} = \frac{d}{dt}\iiint_{CV} \rho e dV + \iint_{CS} \rho e(\vec{v} \times \vec{n}) dA = \sum \vec{M} \tag{15}$$

  In this equation Q stands for heat transferred and W for work.

From the latter theorem we derive Bernoulli's equation, which is highly relevant in fluid mechanics:

$$\frac{p_1}{\rho g} + \frac{v_1^2}{\rho g} + z_1 = \frac{p_2}{\rho g} + \frac{v_2^2}{\rho g} + z_2 = cte \tag{16}$$

This equation states that, under certain conditions of the fluid, its energy remains constant along its path. It can also be deduced from it that the pressure in a flow increases as its velocity decreases and vice versa.

4.2.4 Navier-Stokes Equations

The Navier-Stokes equations are a set of three-dimensional, non-linear partial differential equations governing the dynamic behaviour of fluids.

They are derived from the equation of linear motion and developing the stress tensor. Following the development that can be found in numerous fluid mechanics papers, the following equation is obtained:

$$\rho\vec{f_m} - \vec{\nabla}p + \mu\nabla^2\vec{v} = \rho\frac{D\vec{v}}{Dt} \tag{17}$$

Which developed on Cartesian axes would give:

$$\begin{aligned}
\rho g_x - \frac{\partial p}{\partial x} + \mu\left(\frac{^2u}{\partial x^2} + \frac{^2u}{\partial y^2} + \frac{^2u}{\partial z^2}\right) &= \rho\left(\frac{\partial u}{\partial t} + \frac{\partial u}{\partial x}u + \frac{\partial u}{\partial y}v + \frac{\partial u}{\partial z}w\right)\vec{i} \\
\rho g_y - \frac{\partial p}{\partial y} + \mu\left(\frac{^2v}{\partial x^2} + \frac{^2v}{\partial y^2} + \frac{^2v}{\partial z^2}\right) &= \rho\left(\frac{\partial v}{\partial t} + \frac{\partial v}{\partial x}u + \frac{\partial v}{\partial y}v + \frac{\partial v}{\partial z}w\right)\vec{j} \\
\rho g_z - \frac{\partial p}{\partial z} + \mu\left(\frac{^2w}{\partial x^2} + \frac{^2w}{\partial y^2} + \frac{^2w}{\partial z^2}\right) &= \rho\left(\frac{\partial w}{\partial t} + \frac{\partial w}{\partial x}u + \frac{\partial w}{\partial y}v + \frac{\partial w}{\partial z}w\right)\vec{k}
\end{aligned} \tag{18}$$

This is a system of nonlinear partial differential equations of second order with four unknowns. To solve it, we will need a fourth equation, which is the continuity equation.

To date, no one has been able to solve it completely. It is such a complex system of differential equations involving so many variables that the only way to obtain a solution is numerically or by making numerous simplifications : stationary flow and therefore the time derivatives disappear, ideal flow and therefore the viscous term disappears or two-dimensional problem and the component corresponding to z disappears.

4.3 Fluid Around Solids

In this part of fluid mechanics, the behavior of a moving solid in a fluid is studied. For this purpose, the solid will be imagined as fixed and the uniform flow will be directed towards the object.

4.3.1 Boundary Layer

The boundary layer is the zone of the fluid where its motion is disturbed by the presence of the solid it is in contact with. This phenomenon is due to the no-slip condition and the viscosity of the fluid. The boundary layer is one in which the velocity of the fluid with respect to the moving solid varies from zero to 99% of the velocity of the undisturbed stream.

The thickness (σ) of the boundary layer is the distance from the surface at which the stream velocity is reached. This is increasing, and usually of small extent, depending on the geometry of the object and the Reynolds number; although there may be boundary layer detachment and transient wake formation, which may cover a wide region from the point of detachment.

In this zone of the flow, the viscous effects (τ) of the fluid are present. Outside this boundary layer, the fluid is considered to be ideal.

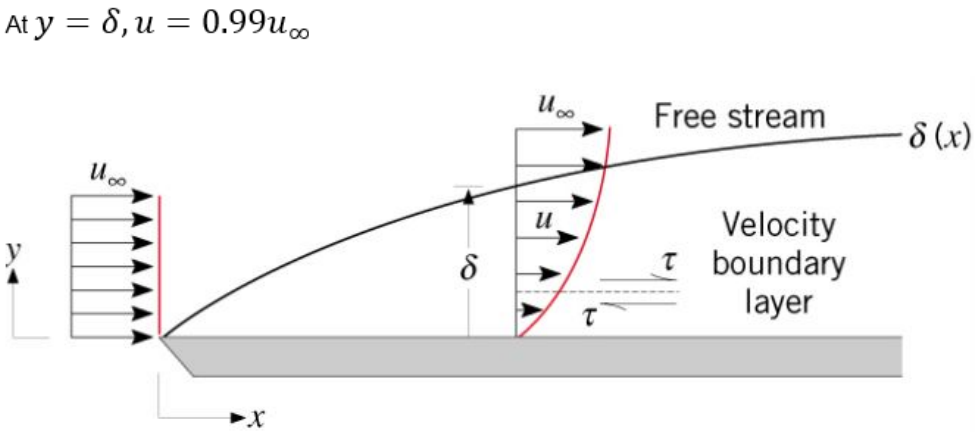

Figure 12: Velocity and boundary layer thickness diagram [Alt].

4.3.2 Aerodynamic Forces and Airfoils

The following picture shows the most relevant parts of an airfoil to which reference will be made throughout this report.

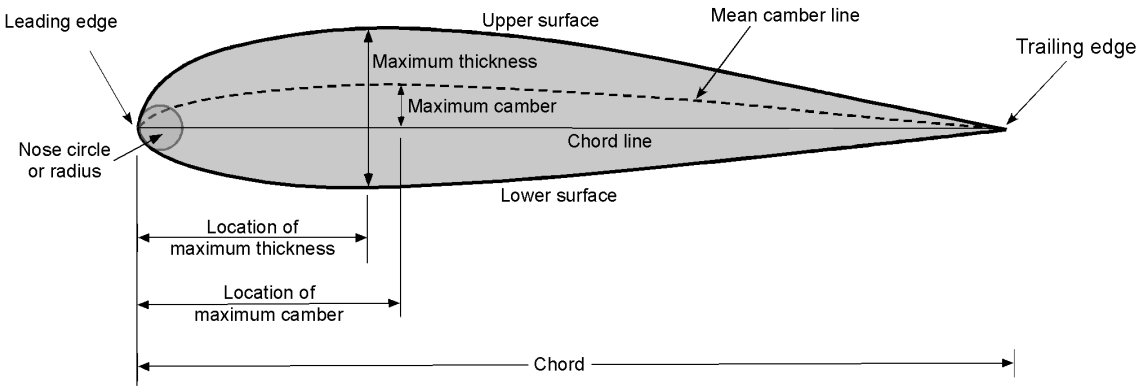

Figure 13: Usual shape and main Parts of an airfoil [ER22].

Another important parameter is the angle of attack, which is the angle formed by the chord of the airfoil with the incident current. This parameter has a decisive influence on the forces generated in the airfoil, as we shall see below.

There are many types of airfoil series already designed. Among the best known and oldest of these is the NACA (National Advisory Committee for Aeronautics) series [ER22]. The NACA airfoil profiles are characterized by a four-digit or five-digit number. The four-digit NACA airfoil designation (e.g., NACA 2412) provides key information about the airfoil's shape:

- The first digit indicates the maximum camber (curvature) as a percentage of the chord length (the distance from the leading edge to the trailing edge).
- The second digit indicates the location of the maximum camber, also as a percentage of the chord length.
- The last two digits indicate the maximum thickness of the airfoil, again as a percentage of the chord length.

The actions of the air on an airfoil (or any other solid) moving with respect to it give rise, at each point on the surface of the body, to a shear stress tangent to the surface due

to the viscosity and a perpendicular stress due to the pressure. Thus, a distribution of pressure and a distribution of shear forces on the surface of the body are obtained, which give rise to the aerodynamic forces.

Lift Force

Lift is the force generated on a body moving through a fluid, perpendicular to the direction of the incident flow.

This force is generated due to the difference in pressures between the lower and upper surface of a body. For example, in airfoils, the velocity of the air flowing through the intrados and extrados is different. This is due to the different curvature of the surfaces and the continuity of the flow. On the longer surface of the airfoil, the flow velocity will be higher than on the shorter side. Therefore, according to Bernoulli's principle (Equation 16), the pressure on the long side will be lower than on the short side. This difference in pressure is the reason for the lift force.

One way to increase the lift force of the same airfoil is to use the angle of attack. As the angle of attack increases, so does the force.

To define the lift experienced by an airfoil or to compare several airfoils, a dimensionless number known as the lift coefficient C_L is used.

$$C_L = \frac{2L}{\rho v^2 S} \tag{19}$$

L is the lift force experienced by the body and S is the reference surface. For ailerons, the area viewed from above is used as the reference surface.

The dependence of lift on angle of attack can be measured by the lift coefficient C_L whose variation with angle of attack α is illustrated in the figure.

The critical or maximum angle of attack is the angle of attack that produces the highest coefficient of lift. It is also called the stall angle of attack. For, above this, as the angle of attack increases, the coefficient of lift begins to decrease. This phenomenon is caused by the fact that the higher the angle of attack, the less able the airflow is to follow the contour of the airfoil.

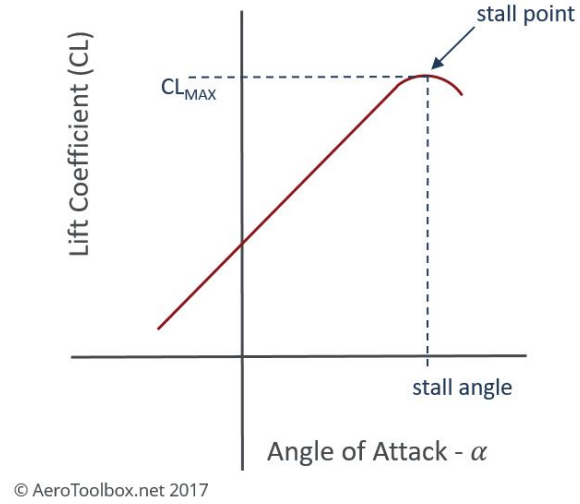

Figure 14: Evolution of lift coefficient in relation to angle of attack.

Resistance or Drag Force

Drag is the force exerted on the body parallel to the direction of the incident current. This force opposes the advancement of the body and in ailerons is the result of several phenomena:

- Drag due to fluid friction: Air is a viscous fluid, and therefore generates tangential forces to the surface of the airfoil, opposing its advance.
- Drag due to the distribution of pressures: this is due to the difference in pressure between the front (overpressure) and the rear (underpressure) of the wing. This generates a force that goes from the area of higher pressure to the area of lower pressure and opposes the aifoil's advance.
- Drag due to the generation of lift or aerodynamic load: Known as induced drag, it appears in bodies that generate lift forces.

As with the lift force, the dimensionless drag coefficient is useful for defining the resistance to which a body is subjected.

$$C_D = \frac{2D}{\rho v^2 S} \tag{20}$$

D is the lift force experienced by the body and S is the reference surface.

The drag coefficient of an airfoil also varies with the angle of attack. An increase in angle of attack is associated with an increase in the coefficient of drag.

5 Work Methodology and Resources to be Used

In order to achieve the objectives previously established for this Final Degree Project, the following stages will be carried out:

5.1 Wing Design Steps

5.1.1 Choice of Airfoils

The first step to be taken is to determine the airfoils to be used in the wing. To do this, a study will be carried out and aerofoils will be selected in accordance with the objectives of this Final Degree Project.
Subsequently, a CFD analysis of these airfoils with different angles of attack will be carried out. This will enable to choose which airfoils and with which angle of attack will act as a possible main element and which will act as a flap.

5.1.2 Configurations Analysis

Secondly, different proposals for the final aileron will be designed on the basis of the aerofoils selected in the previous stage. CFD analysis of these configurations will then be carried out to determine the most efficient one.

5.1.3 Analysis of Results and Conclusions

Finally, the design chosen at the previous stage will be analysed. Its strengths and weaknesses will be presented, followed by improvements that could be made to reduce the latter. Also, future work that could be done on the basis of this first design will be discussed.

5.2 Resources to be used

In order to proceed with the steps outlined above, three main tools will be used.

The CAD design of the aileron will be carried out in SolidWorks, a 3D CAD design software. This program offers several solutions that are adapted to the objectives of this Final Degree Project. The design tools for creating models and assemblies will allow the design of the spoiler to be carried out and coupled with the design of the rest of the single-seater. The design tools for mechanical manufacturing will allow the generation of 2D drawings useful for the subsequent manufacture of the wing.

Although SolidWorks also has fluid dynamics analysis software, the CFD package ANSYS-FLUENT will be used for this task. This is the leading fluid simulation software in the sector, and is the most widely used for this type of project.

CFD ANSYS-FLUENT will allow to carry out all the stages set out in the previous section in order to achieve the objectives of this Final Degree Project. The 'Student' version of this software will be used, which has some limitations with respect to the general licence. For instance, the mesh will have to contain a maximum of 512000 elements, which will be sufficient for our simulations.

Finally, the online tool airfoiltools.com will be used. This reliable website provides access to a large database containing a wide variety of aerofoils. It also allows the generation of profiles with specific characteristics. This tool will be used to extract the coordinates of the airfoils which will then be entered into the CAD software for the design.

6 Aerofoils Performance Analysis

This section presents the CFD analysis of the individual airfoils and the following selection of the most performant ones.

Three different types of airfoils are chosen and designed in Solid Works to later carry out a CFD analysis of each one with different angles of attack. This will allow to establish their optimal position and thus identify whether they will act as a main or secondary element (flap) in the final aileron.

6.1 Preliminary Decisions

Before starting with the CFD simulations for the choice of airfoils, some key parameters for the design of this wing will be defined.

The first decision to be made is the type of wing to be designed. As discussed above, this can be a single or multi-element wing. The most efficient in terms of performance would be to install a 3-element wing, as other formula student teams do. However, due to the recent creation of the team and therefore low financial resources, a two airfoil wing will be built, trying to ensure maximum aerodynamic efficiency.

The dimensions will then be chosen, which will have to be in accordance with the Formula Student 2023 regulations. When determining these dimensions, it has to be taken into account that the larger the wing is, the more effective it will be, i.e. the more negative lift force it will create. The force generated towards the ground is the result of a difference in pressure on the upper and lower surfaces, so the larger the aileron surface in contact with the airflow, the greater the force.

As a consequence of this, the largest measurements allowed by the formula student regulations will be taken:

- Width: As this is an aerodynamic element that will be more than 0.5 metres above the ground, it cannot extend beyond the inside plane of the tyres. The distance between the tyres of the ApeCS single seater is 645mm. For the width of the profiles, a measurement with a certain margin will be taken to avoid problems such as chassis changes that modify the tyre spacing. Also, the addition of endplates will

increase the width, albeit minimally. Therefore, the width of the spoiler airfoils will be 610mm.

- Chord: This parameter is also influenced by the regulations. As we have seen before, no aerodynamic element of the car may exceed 250mm from the rearmost plane of the wheels. Taking into account that the wing will be installed from the frontmost plane of the tyres, the total chord of the wing will be 450mm, which will be divided between the chords of the two aerofoils.

  As previously mentioned, the maximum aileron efficiency will be for a 25%c-30%c apportionment for the flap chord (where $c = 450mm$). As we will see later, in the individual airfoil analyses, CFD problems will be calculated for an average value of 32%c (=324mm) for the main airfoil chord and 28%c (=126mm) for the flap chord. In the analyses of the possible configurations, the most efficient distribution between 25%c and 30%c will be evaluated.

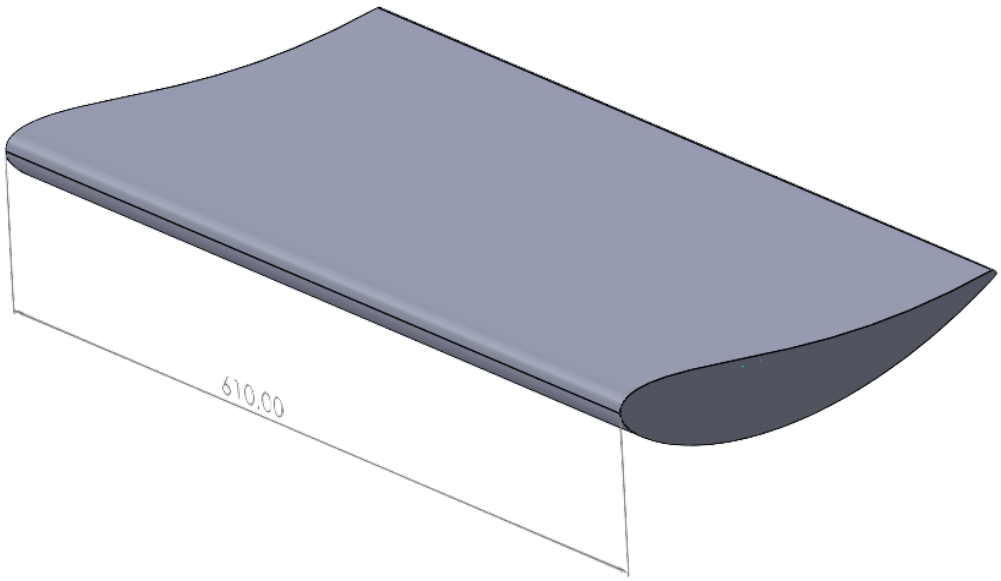

Figure 15: Representation of the width set for all wing profiles.

6.2 Aerofoil Selection

In this section, the airfoils to be analysed will be selected for possible use in the rear wing of the ApeCS single-seater. The airfoils to be chosen should not exhibit very complex shapes in order to facilitate their subsequent construction.

In order to evaluate different series of airfoils, the following ones have been selected:

- **NACA 9517**: In his book Competition Car Aerodynamics, Simon McBeath simulated a 632-615 airfoil in 2D CFD, and analysed how the negative lift force behaved when varying different airfoil properties such as angle of attack, camber and thickness. As a result, he determined the following optimum characteristics:

	McBeath Recommendation
Camber	9%c at 50%c
Thickness	18%c higher downforce 16%c higher efficiency

Table 3: Summary of the characteristics of an optimal NACA profile according to McBeath [McB15].

Where c is the length of the chord

Therefore one of the selected airfoil will be NACA 9517, with the camber recommended by McBeath (9%c to 50%c) and the intermediate thickness between the two presented (17%c).

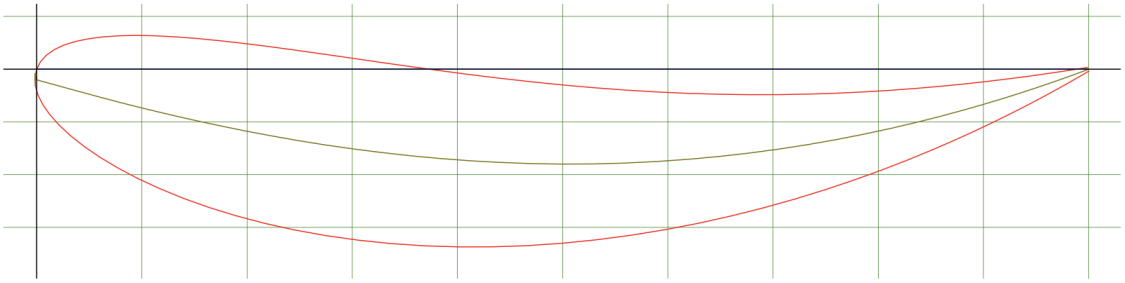

Figure 16: NACA 9517 aerofoil shape [Air].

- **GOE 447**: It is known that nowadays GOE airfoils are one of the basics when starting to design in competitions like Formula 1. Despite the fact that the current ailerons are very different from the basic profiles.

For this reason, and due to its non-complicated geometry, it was decided to study the GOE 447 aerofoil from this series.

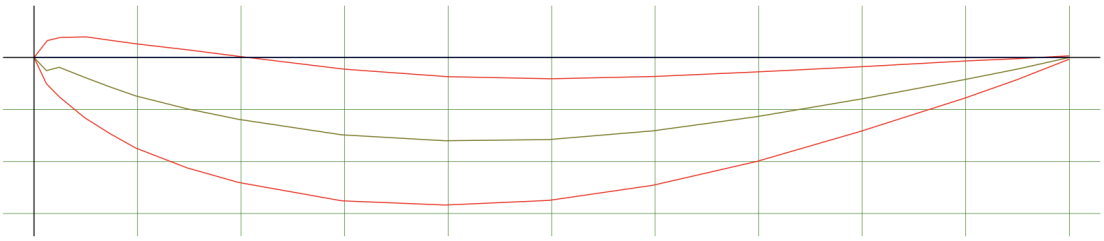

Figure 17: GOE 447 aerofoil shape [Air].

- **e423**:Finally, it is decided to analyse a aerofoil with a slightly more complex shape than the others. It is similar to the profile presented above, but with a little more curvature on the upper face, which could make it harder to manufacture. With this airfoil, the aim is to evaluate whether it is worth using an airfoil with a more complicated shape in relation to the aerodynamic load it generates. E-423 is chosen because it is known to generate downforce at low speed.

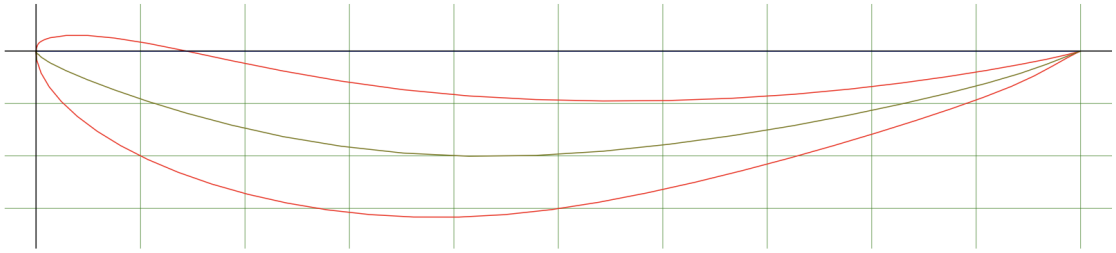

Figure 18: E423 aerofoil shape [Air].

The three airfoils will then be evaluated with different chords and angles of attack to determine their optimal function.

6.3 Airfoil CAD Design

The 3 ailerons chosen in the previous step were designed in CAD format. For this purpose, as mentioned above, the airfoil coordinates extracted from airfoiltools [Air] were used. However, the curvature of the trailing edge of the ailerons had to be modified to meet the regulations for the minimum radius of the aerodynamic elements.

In addition, the coordinates are given for airfoils that generate positive lift. As the opposite effect is sought in this project, it is sufficient to oppose the y-axis coordinates.

(a) NACA 9517

(b) GOE 447

(c) E-423

Figure 19: Final aileron shapes with modified trailing edge to meet Formula Student restrictions.

6.4 Simulation Process

For the development of all the simulations with Ansys Fluent, the stages established by the software itself have been followed:

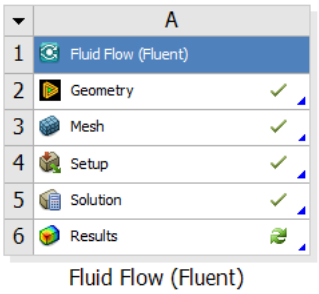

Figure 20: Fluent steps to follow to carry out CFD simulation.

6.4.1 Geometry

In this step the study profile is generated. First, the file containing the part to be studied, previously designed in Solid Works, is imported. In all cases, given the longitudinal symmetry of the models to be analysed, it is decided to simulate one of the halves. This is to save both effort and computational time. It can be assumed that the results of one half are identical to those of the other half.

Next, in this same step, the control volume that simulates what a wind tunnel would be like is defined. In order that the walls of this volume do not affect the study of the forces in the geometry to be analysed, it must have certain dimensions depending on the component under study.

	Recommended dimension
In front of the model	$\geq 2\times$ model length
Behind the model	$10\times$ model length
Height	$5\times$ model height
Width	$10\times$ model width

Table 4: Recommended dimensions of the control volume and used in all the simulations of this thesis.

6.4.2 Meshing

The meshing process is one of the key parts of the simulation. This stage aims to divide the air box into a number of sub-regions. By dividing the control volume into sub-regions you are approximating the model to what it would look like in reality. Thus, the higher the number of elements, the better the quality of the mesh and the better the results.

In this project, the Ansys 'Student' licence is used, so the number of 512000 mesh elements is limited to 512000. As the geometries are not very complex, this number of elements is sufficient for the optimal calculation of the objectives of this project. However, 512000 meshes will be used in all simulations to ensure maximum accuracy.

In addition, in this procedure, the different bodies and surfaces of the geometry are named. This will be useful to define in the next stage the boundary conditions and to determine from which surfaces the data should be collected.

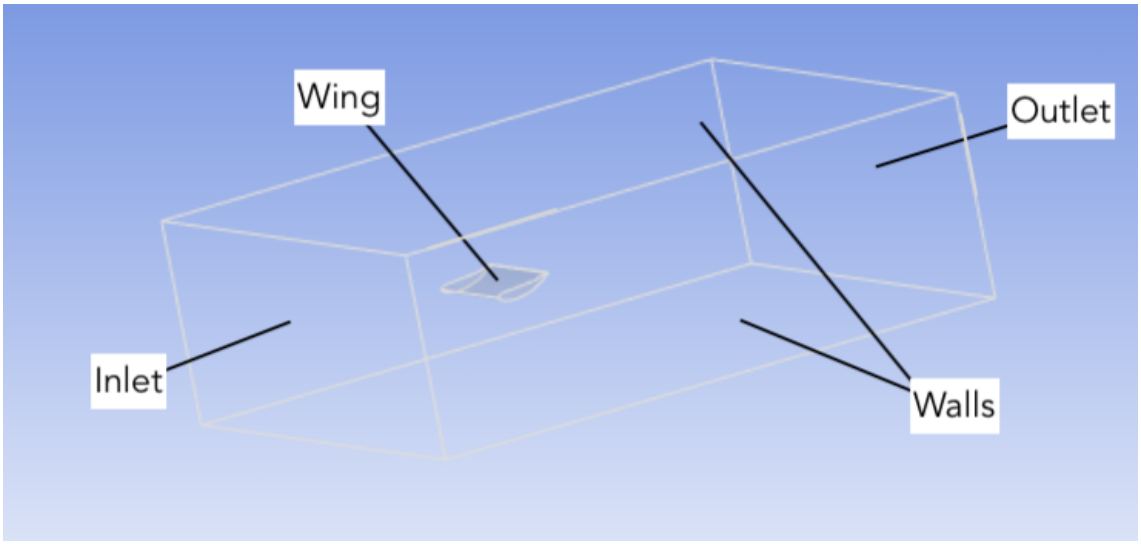

Figure 21: Example of bodies and surface definition in a simulation of a NACA 9517 airfoil.

In the image shown above, the symmetry plane created in the previous step, which divides the aileron in half, remains to be defined.

6.4.3 Set Up

It is in this last stage where the parameters necessary to solve the problem, such as the properties of the fluid, the boundary conditions, etc., are configured.

The first step is to determine the turbulence model. The model commonly used to model turbulence for ground vehicles is the two-equation model $k - \epsilon\, Realisable$ and without wall equilibrium functions. The objective of this model is to simulate the properties of the turbulent flow, thanks to two transport equations:

- Turbulent kinetic energy (k)
- Turbulent dissipation (ϵ)

Next, the working fluid is determined. This will be the air surrounding the vehicle. In the software's database, a density value of 1.25 kg/m3 and a kinematic viscosity of 1.7894 kg/ms are established.

Then the boundary conditions are set. These will be specified in the zones named in the previous meshing step. The conditions set in all simulations are listed below:

- Inlet velocity: a velocity of 17 m/s is set on the face named above as inlet. This speed is chosen as it is the average for Formula Student vehicles.
- Outlet pressure: a pressure of 0 Pa is set on the outlet surface. This pressure is selected because the outlet of the wind tunnel is at ambient pressure, so the relavitve pressure is equal to 0.
- In the defined plane defined as 'Symmetry' no parameter conditions are needed, the software knows the function of a symmetry plane.
- The rest of the planes are set up as stationnary walls, as they have no movement.

Finally, the forces to be calculated during the simulation are configured; for this work, lift and drag are relevant. Although they can be calculated once the case has converged, it is convenient to do so at each iteration, as it can help determine the point where the simulation converges (when its values stabilise).

Once everything is set up, the simulation is initialised. To do so, a hybrid initialisation will be selected. The program will solve fifteen iterations starting from the assumption of constant pressure throughout the fluid domain. The result of the fifteenth iteration will serve as the starting point for the simulation.

Once the problem has been initialised, the number of iterations is indicated and the calculation is executed.

6.5 GOE 447 Results

The behaviour of this airfoil will be studied both for the main element and for the secondary or flap. On the one hand, the aerofoil designed for the main plane with chord $72\%c = 324mm$ will be evaluated for different angles of attack between 0^{o} and 25^{o}. On the other hand, the airfoil designed for flap with chord $28\%c = 126mm$ will be evaluated for angles of attack between 15^{o} and 35^{o}. In order to reduce the computational time, the analyses will be carried out for 5^{o} intervals, and then further analyses will be carried out in order to deepen the most interesting points of the results obtained.

6.5.1 GOE 447 326mm Chord

The results obtained for lift, drag and lift over drag of the GOE 447 airfoil as the main element of the wing (326mm chord) are shown in the table 4 and the figures 22, 23 and 24.

Angle of Attack	C_L	C_D	C_L/C_D	F_L	F_D
0°	-0,34530421	0,043050216	-8,020963472	-11,55838983	1,441022625
5°	-0,60263196	0,076478377	-7,879769206	-20,0951777	2,550224147
10°	-0,86237924	0,13088808	-6,588676677	-28,42792866	4,314664393
15°	-1,1613244	0,2159984	-5,376541678	-37,5485174	6,983767568
20°	-1,4608022	0,32679722	-4,470056997	-45,94864357	10,27920754
25°	-1,7612963	0,46394755	-3,79632633	-53,43226679	14,07472966

Table 5: Results obtained from the CFD calculation of the GOE 447 324mm chord airfoil.

Figure 22: Representation of the lift coefficient with respect to the angle of attack of the GOE 447 airfoil with a chord of 324mm.

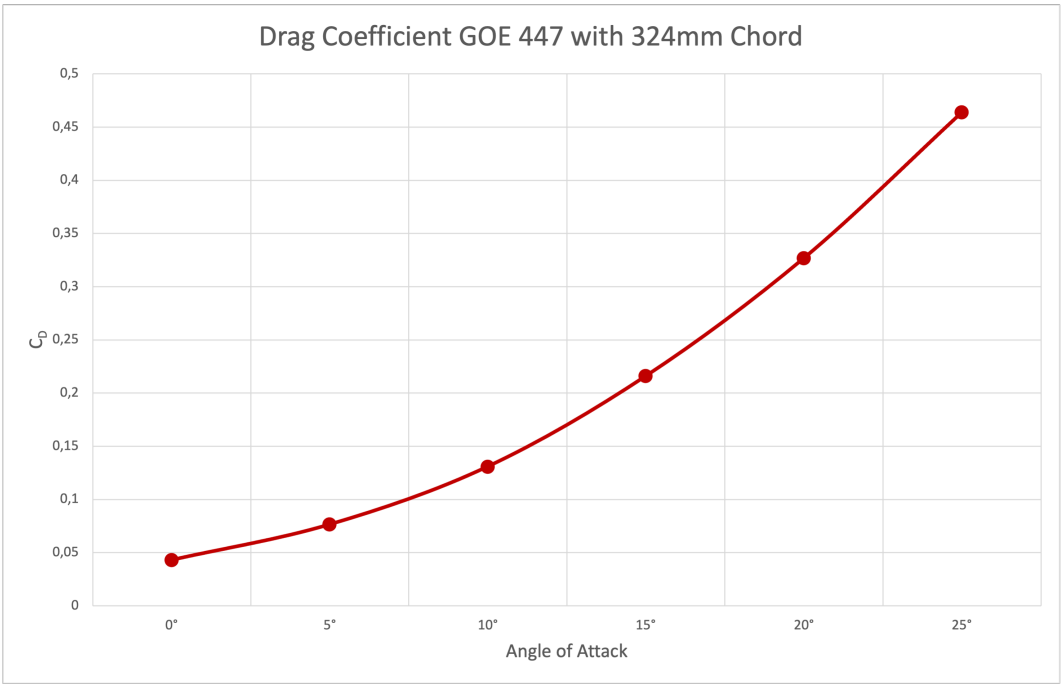

Figure 23: Representation of the drag coefficient with respect to the angle of attack of the GOE 447 airfoil with a chord of 324mm.

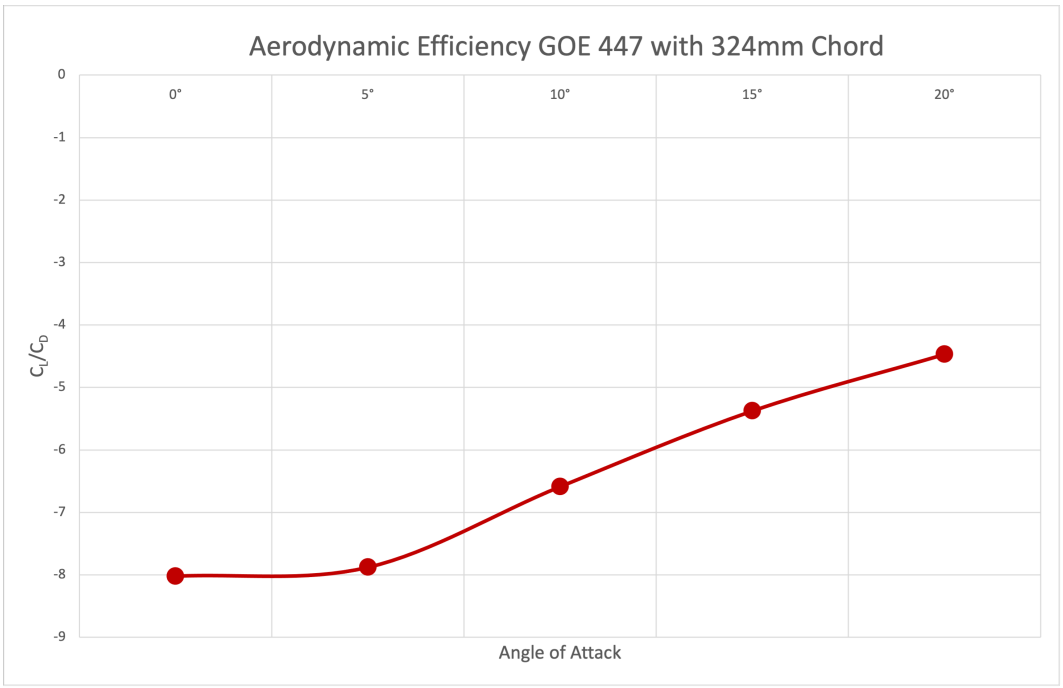

Figure 24: Representation of the aerodynamic efficiency with respect to the angle of attack of the GOE 447 airfoil with a chord of 324mm.

These results reveal what is expected. An almost linear increase in the anti-lift coefficient (negative lift coefficient) can be appreciated as the angle of attack increases. The drag coefficient also rises with increasing angle of attack.

One of the remarkable aspects of these graphs is that for an angle of attack of 5 degrees, although the anti-lift coefficient increases, the aerodynamic drag does not do so as much. This results in an aerodynamic efficiency coefficient almost the same as for 0 degrees.

6.5.2 GOE 447 126mm Chord

CFD analysis of the GOE 447 profile with 126mm chord revealed the following results:

Angle of Attack	C_L	C_D	C_L/C_D	F_L	F_D
15°	-1,2795468	0,14416751	-8,875417214	-16,81528641	1,894591095
20°	-1,5022317	0,20288815	-7,404235782	-19,20556352	2,593861688
25°	-1,6958433	0,27582087	-6,148350196	-20,91056403	3,401004068
30°	-1,6616927	0,3592221	-4,625808657	-19,5787815	4,232510021
35°	-1,3760269	0,49871957	-2,759119519	-15,33542299	5,558085789

Table 6: Results obtained from the CFD calculation of the GOE-447 126mm chord airfoil.

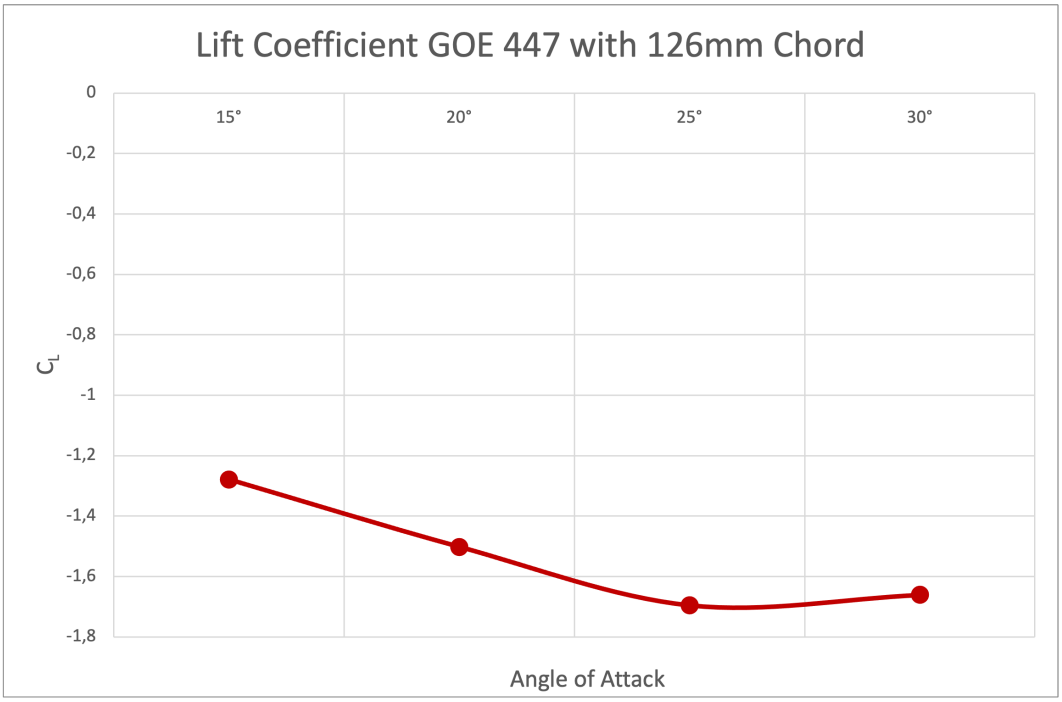

Figure 25: Representation of the lift coefficient with respect to the angle of attack of the GOE 447 airfoil with a chord of 126mm.

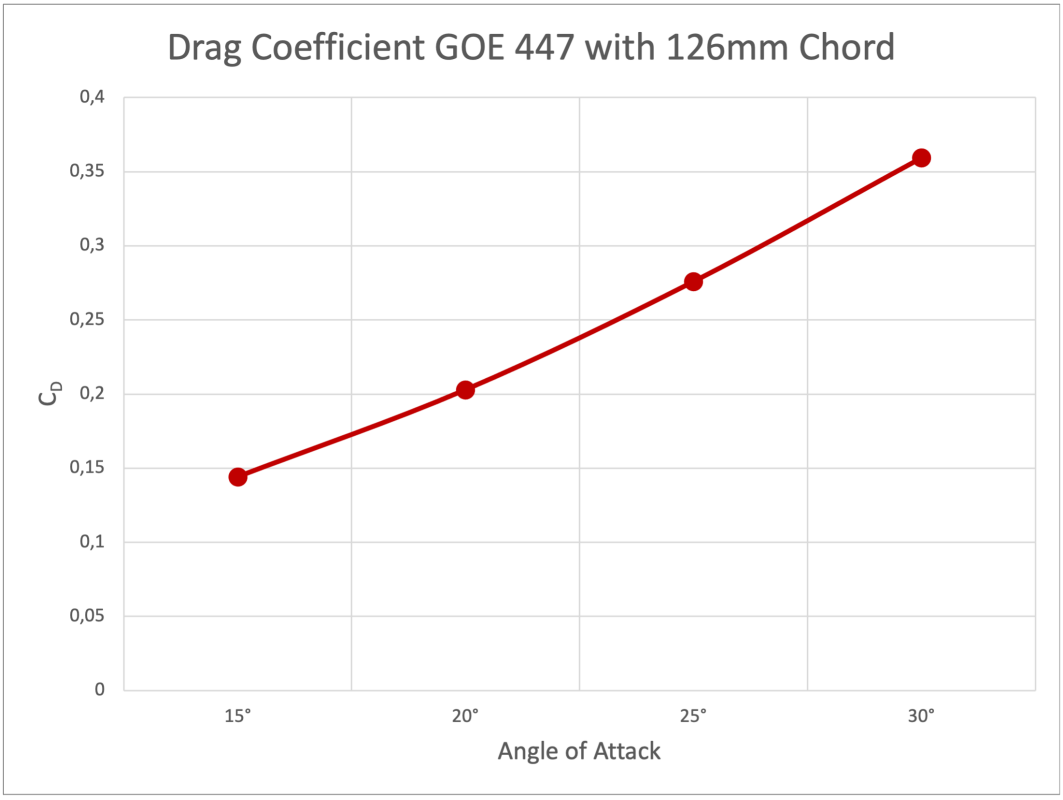

Figure 26: Representation of the drag coefficient with respect to the angle of attack of the GOE 447 airfoil with a chord of 126mm.

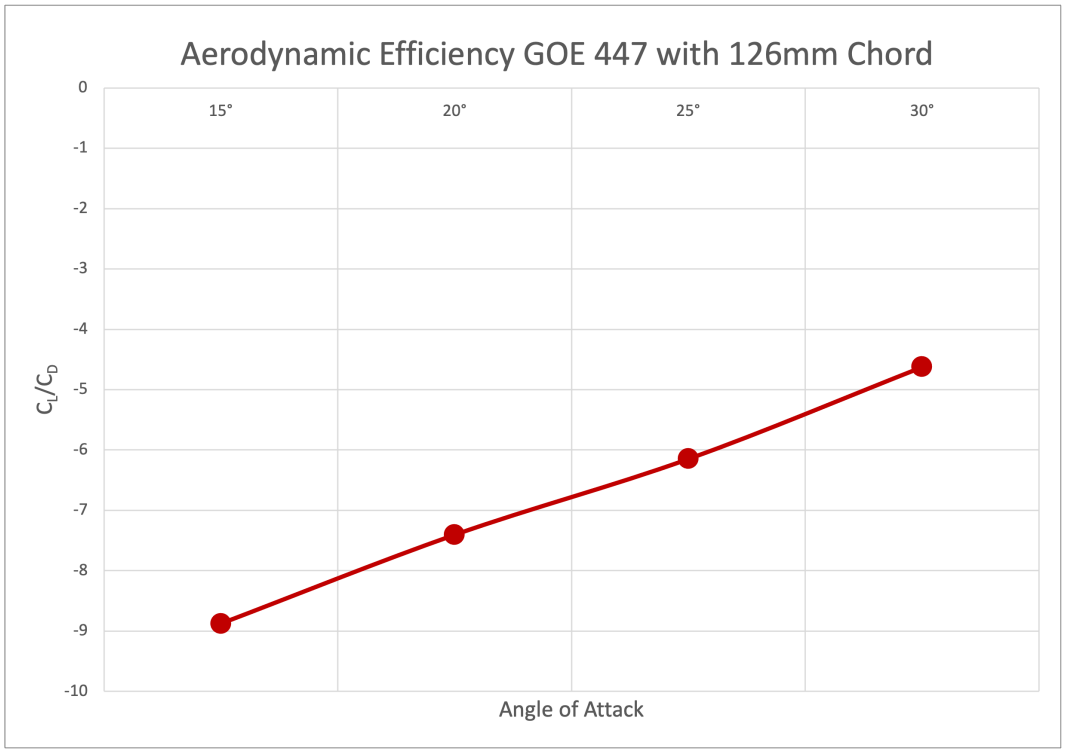

Figure 27: Representation of the aerodynamic efficiency with respect to the angle of attack of the GOE 447 airfoil with a chord of 126mm.

The graphs displaying the results show that the GOE 447 airfoil with a 126mm chord stalls at an angle of approximately 25 degrees. This means that the airfoil reaches the maximum lift it can generate and from there onwards, as the angle increases, the lift will decrease. As seen before, this is due to the detachment of the boundary layer. For this reason, when choosing, this profile will only be taken into account for an angle of less than 25 degrees.

6.6 E-423 Results

For this airfoil, the same procedure as for the previous one shall be carried out. Its performance shall be evaluated for both the main airfoil and the flap. The main airfoil has a chord of 324 mm and the secondary of 126 mm.

6.6.1 E-423 324mm Chord Results

First, the behaviour of E-423 is analysed for a 324mm chord. The results are shown below:

Angle of Attack	C_L	C_D	C_L/C_D	F_L	F_D
0°	-0,41511967	0,056106532	-7,398776135	-13,89532718	1,878057522
5°	-0,6688797	0,091786483	-7,28734426	-22,30425421	3,060683483
10°	-0,92392131	0,14968379	-6,172487415	-30,45663423	4,93425619
15°	-1,2155889	0,23744379	-5,119480699	-39,30302417	7,677150571
20°	-1,5238419	0,3550065	-4,292433801	-47,93151895	11,16651326
25°	-1,8386736	0,50085509	-3,671069011	-55,77965407	15,19438994

Table 7: Results obtained from the CFD calculation of the E-423 with 324mm chord.

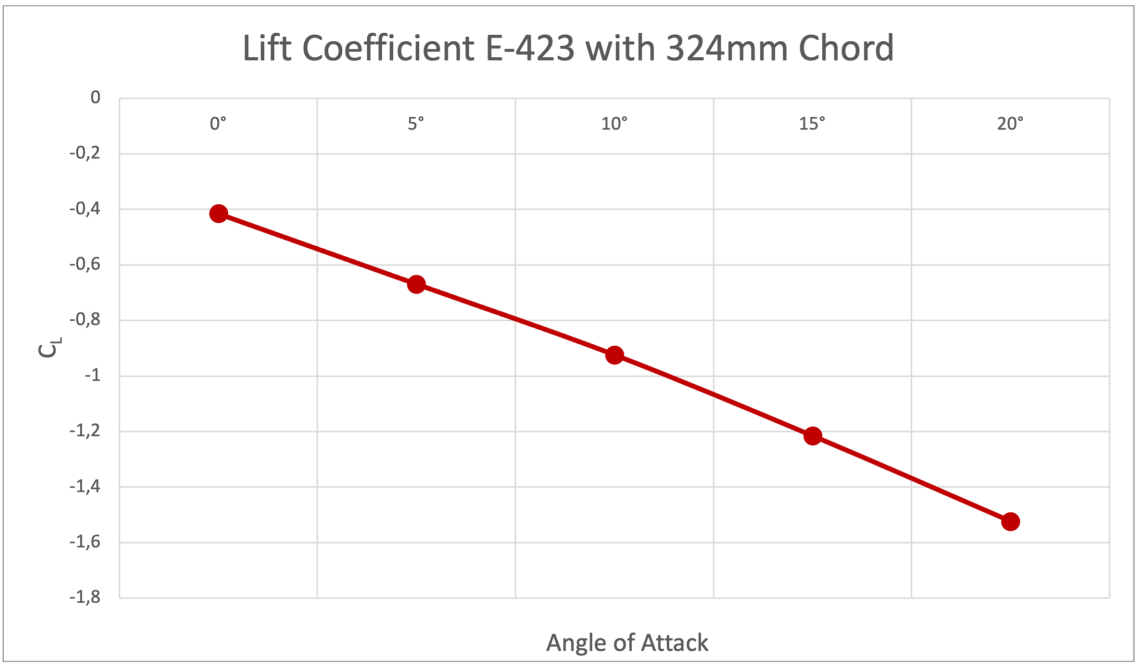

Figure 28: Representation of the lift coefficient with respect to the angle of attack of the GOE 447 airfoil with a chord of 126mm.

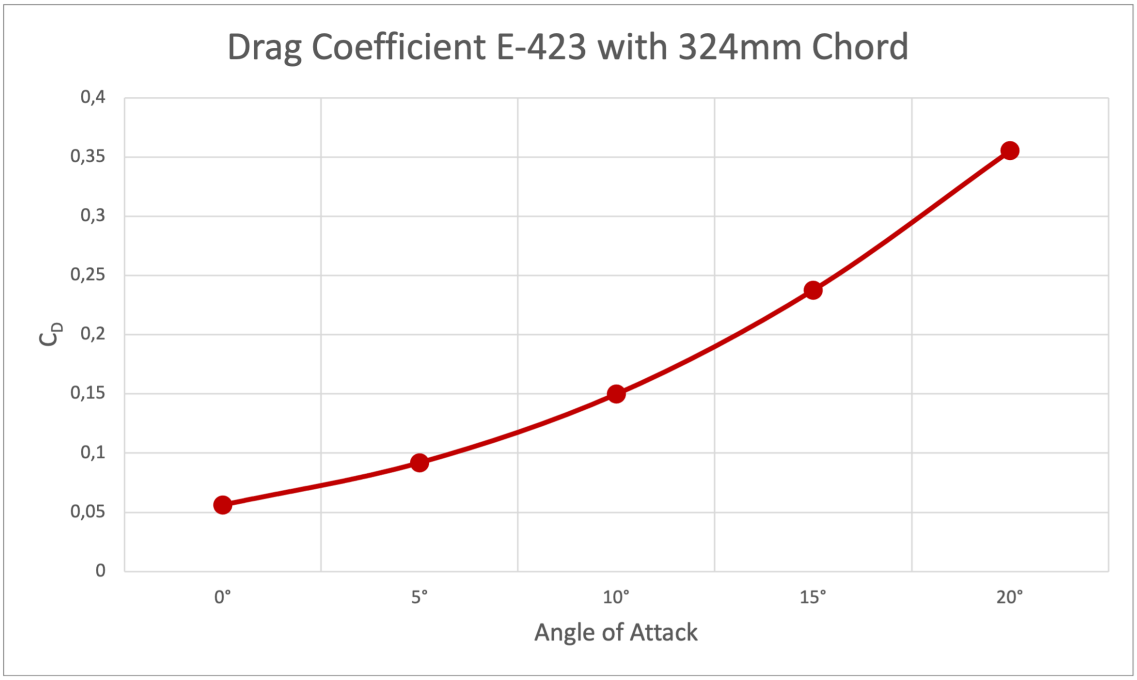

Figure 29: Representation of the drag coefficient with respect to the angle of attack of the E-423 airfoil with a chord of 324mm.

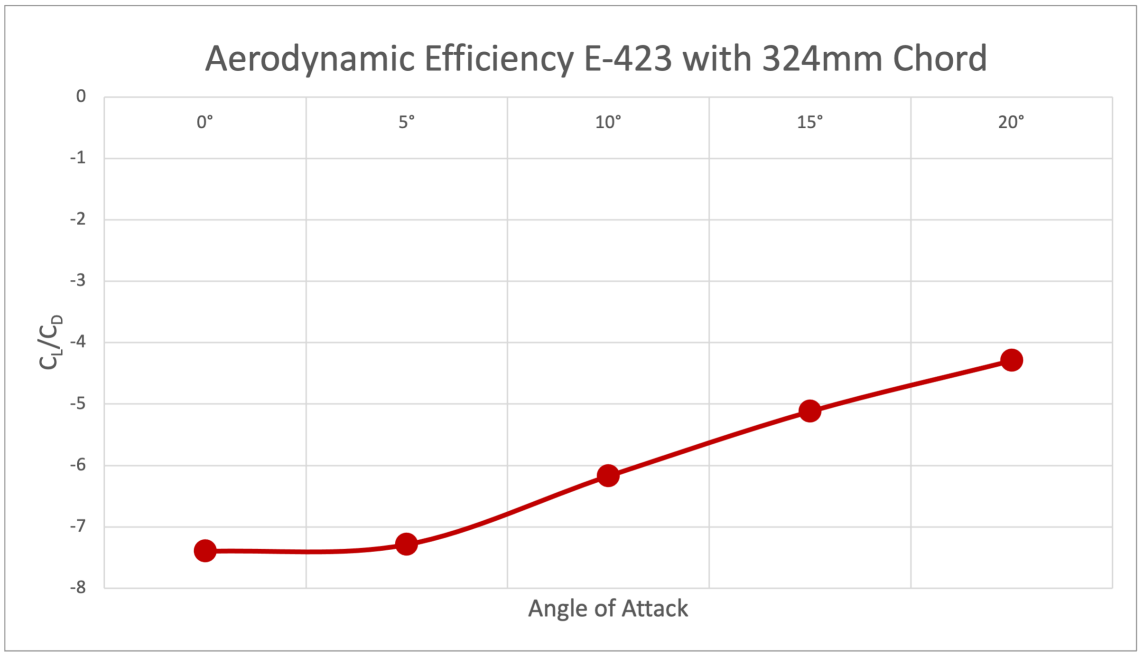

Figure 30: Representation of the aerodynamic efficiency with respect to the angle of attack of the E-423 airfoil with a chord of 324mm.

In this case, the graphs show a close resemblance to the performance of the GOE 447 with a 324mm chord. This is due to the similar geometries. We can see an almost linear increase in the lift coefficient. In addition, it is worth highlighting the similarity of the aerodynamic efficiency coefficient for 0 and 5 degrees, as the lift is increased with hardly any change in drag, which is one of the objectives of vehicle aerodynamics and therefore of this final degree project.

6.6.2 E-423 126mm Chord Results

The results obtained for the E-423 profile with a 126 mm chord are shown below:

Angle of Attack	C_L	C_D	C_L/C_D	F_L	F_D
15°	-1,1773375	0,12443807	-9,461232403	-15,47209314	1,635314775
20°	-1,4283287	0,17689752	-8,074328572	-18,26073673	2,261579593
25°	-1,6607878	0,24349567	-6,820605065	-20,47831284	3,002418795
30°	-1,7248947	0,31249764	-5,519704725	-20,32345477	3,681982241
35°	-1,6412774	0,40991533	-4,003942473	-18,29156332	4,568388143

Table 8: Results obtained from the CFD calculation of the E-423 with 324mm chord.

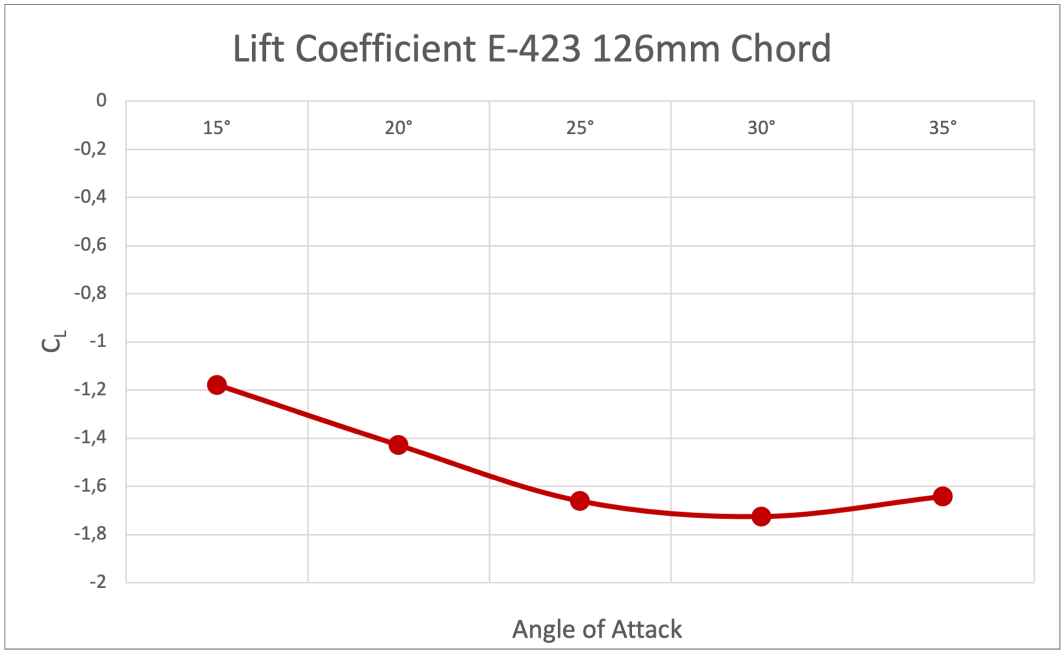

Figure 31: Representation of the lift coefficient with respect to the angle of attack of the GOE 447 airfoil with a chord of 126mm.

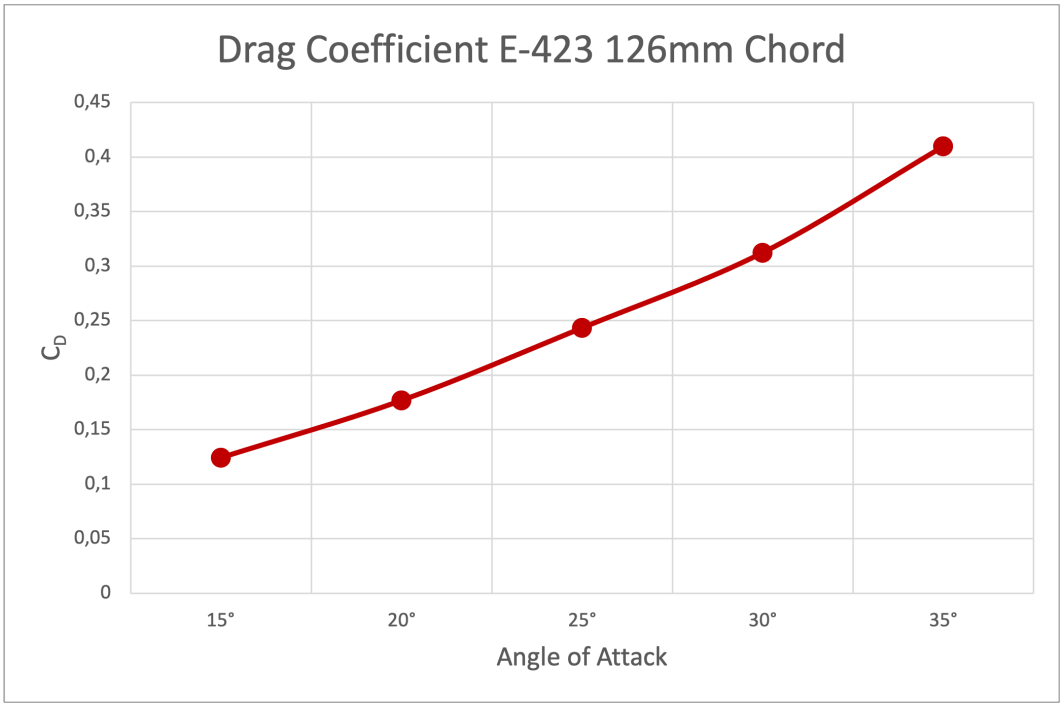

Figure 32: Representation of the drag coefficient with respect to the angle of attack of the E-423 airfoil with a chord of 126mm.

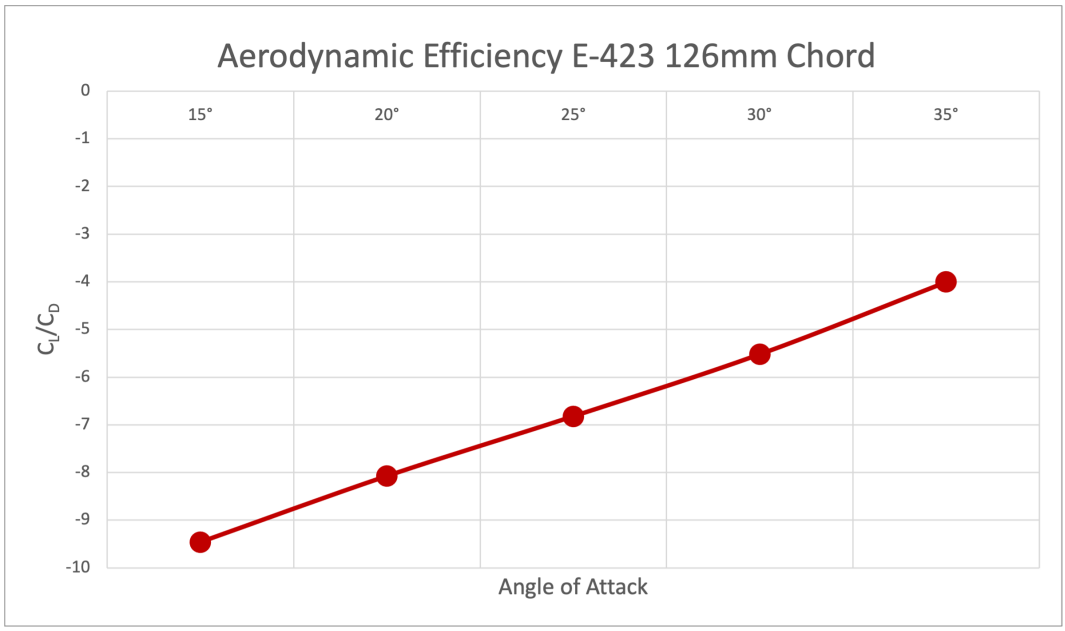

Figure 33: Representation of the aerodynamic efficiency with respect to the angle of attack of the E-423 airfoil with a chord of 126mm.

For the E-423 aerofoil with 126mm chord, it was decided to perform the CFD calculations for angles greater than 30 degrees, as the stall angle had not yet been reached at this point. Thus it can be seen that this is around 30 degrees. This is a larger angle than for the GOE 447, therefore this airfoil will be prioritised over the previous airfoil in the subsequent selection.

6.7 NACA 9517 Results

Finally, the last airfoil chosen for this purpose will be analysed.

The same analysis has been carried out as for the two previous ones, with the same procedure and the same dimensions. The following sections show and analyse the results achieved.

6.7.1 NACA 9517 324mm Chord

The results for the first profile with 324mm chord are presented in the following table and figures.

Angle of Attack	C_L	C_D	C_L/C_D	F_L	F_D
0°	-0,45530464	0,060362447	-7,542845968	-15,24044124	2,020516037
5°	-0,70900239	0,10202428	-6,949349606	-23,64217294	3,402069874
10°	-0,97662631	0,16736703	-5,835237143	-32,19402993	5,517175933
15°	-1,2628221	0,25900631	-4,875642219	-40,83019146	8,374320679
20°	-1,573634507	0,384369227	-4,09406996	-49,49771507	12,09009996
25°	-1,868715269	0,524477513	-3,563003606	-56,69102514	15,91102098

Table 9: Results obtained from the CFD calculation of the E-423 with 324mm chord.

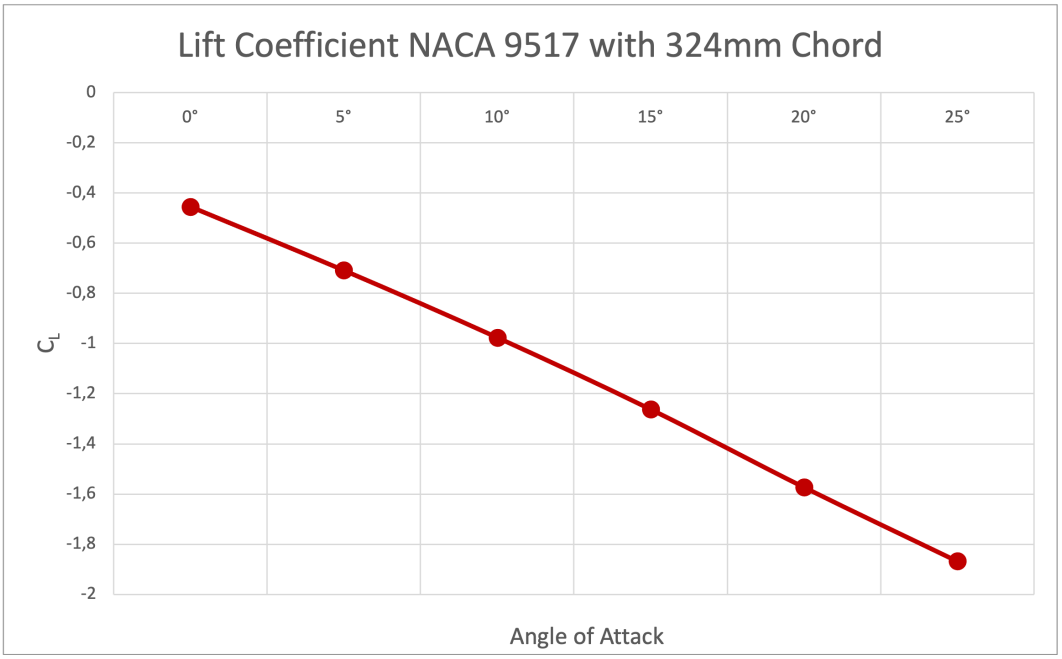

Figure 34: Representation of the lift coefficient with respect to the angle of attack of the NACA 9517 airfoil with a chord of 324mm.

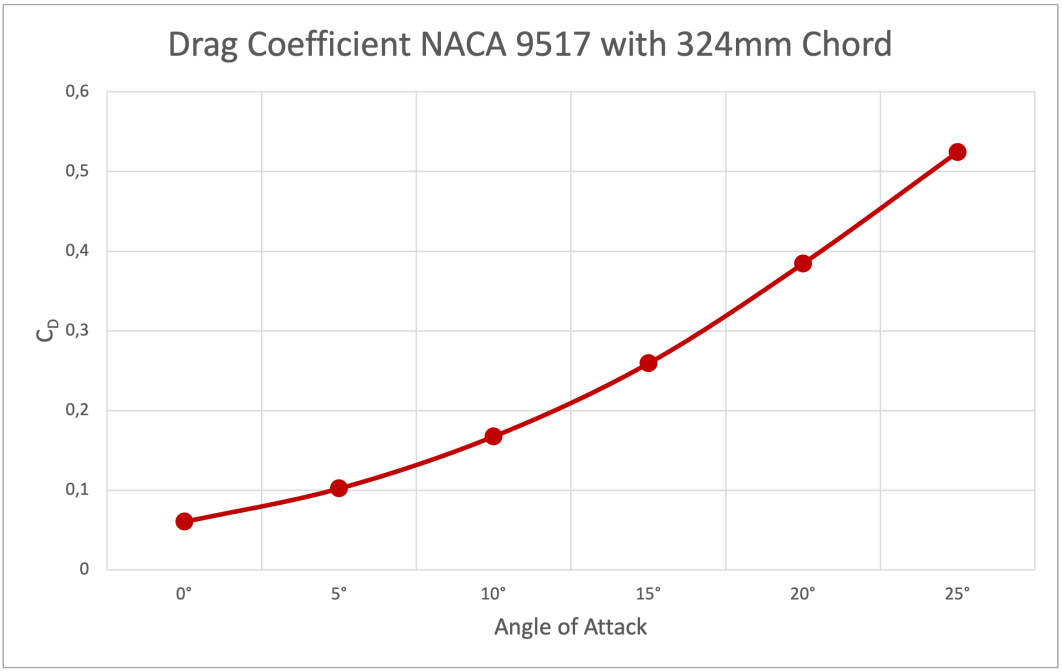

Figure 35: Representation of the drag coefficient with respect to the angle of attack of the NACA 9517 airfoil with a chord of 324mm.

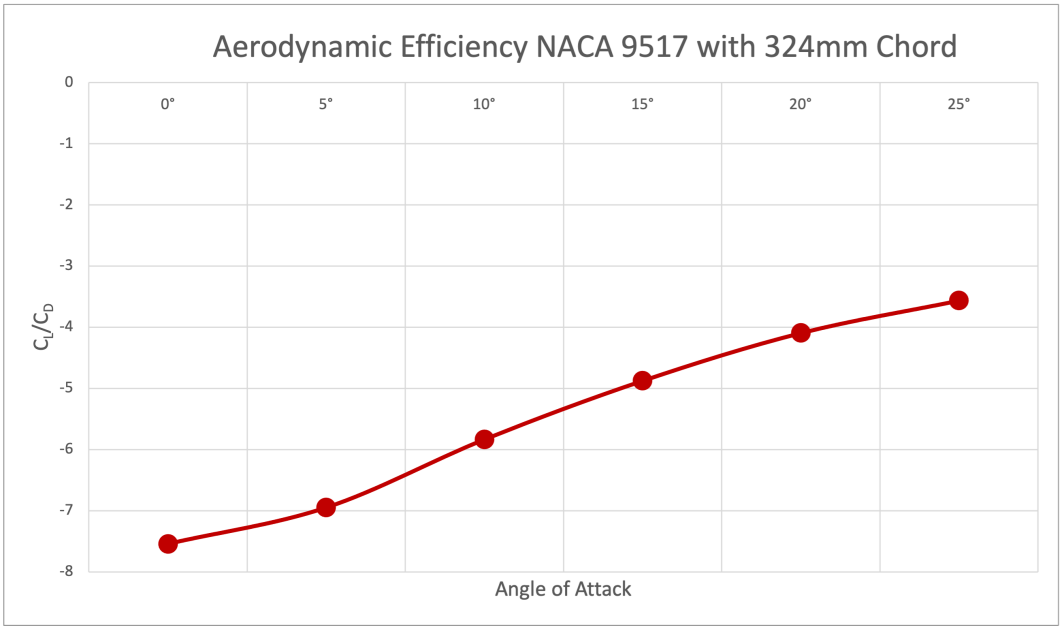

Figure 36: Representation of the aerodynamic efficiency with respect to the angle of attack of the NACA 9517 airfoil with a chord of 324mm.

As in the previous cases, an almost linear increase in anti-lift is observed. As for the aerodynamic efficiency coefficient, it evolves relatively proportionally, except for the 0 to 5 degree range. In this period, the lift increases more than the drag, which is why the CL/CD coefficient is favourable. However, this increase in anti-lift with little growth in drag for this airfoil is less significant than for the other two airfoils.

6.7.2 NACA 9517 126mm Chord

Finally, the results of the NACA 9517 designed to act as a flap will be discussed.

Angle of Attack	C_L	C_D	C_L/C_D	F_L	F_D
15°	-1,3504256	0,15806103	-8,54369733	-17,74674693	2,077174114
20°	-1,6444418	0,22567361	-7,286814794	-21,02367527	2,885166684
25°	-1,8792838	0,30134687	-6,236281133	-23,17247367	3,715751933
30°	-2,0697526	0,38191212	-5,41944728	-24,38671958	4,499853642
35°	-2,0299656	0,47262459	-4,295090952	-22,62338122	5,267264762

Table 10: Results obtained from the CFD calculation of the E-423 with 324mm chord.

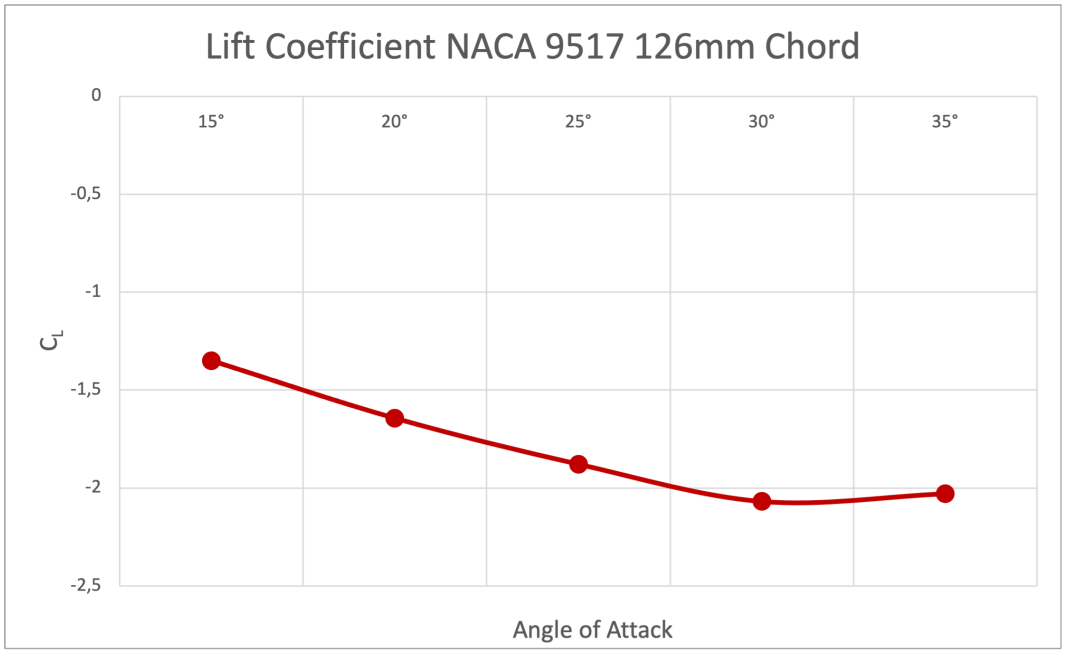

Figure 37: Representation of the lift coefficient with respect to the angle of attack of the GOE 447 airfoil with a chord of 126mm.

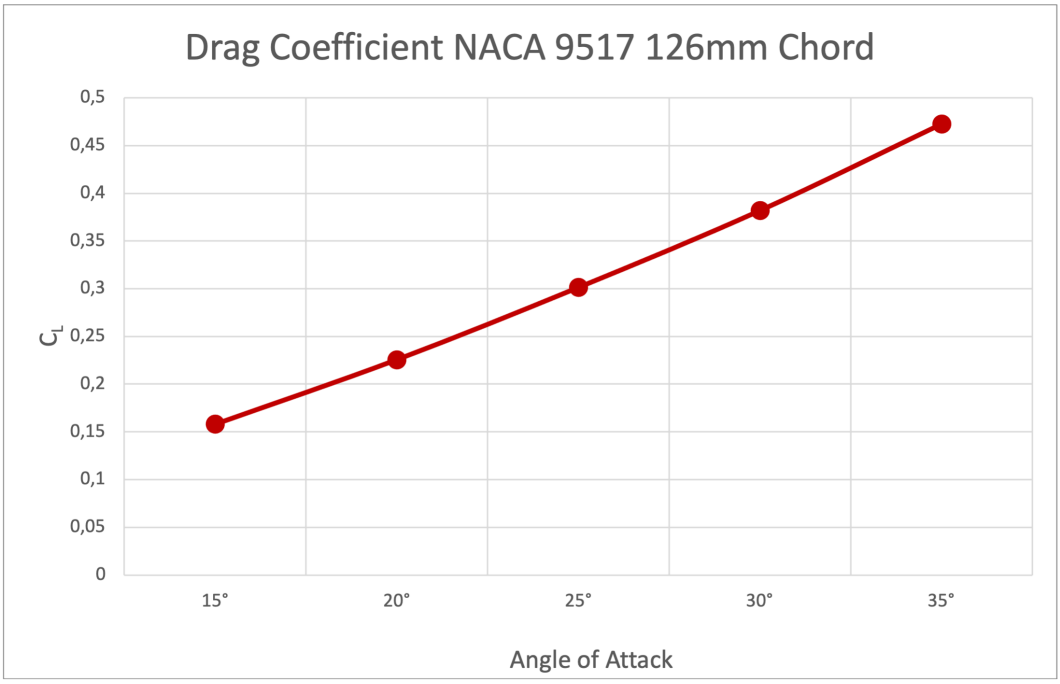

Figure 38: Representation of the drag coefficient with respect to the angle of attack of the E-423 airfoil with a chord of 324mm.

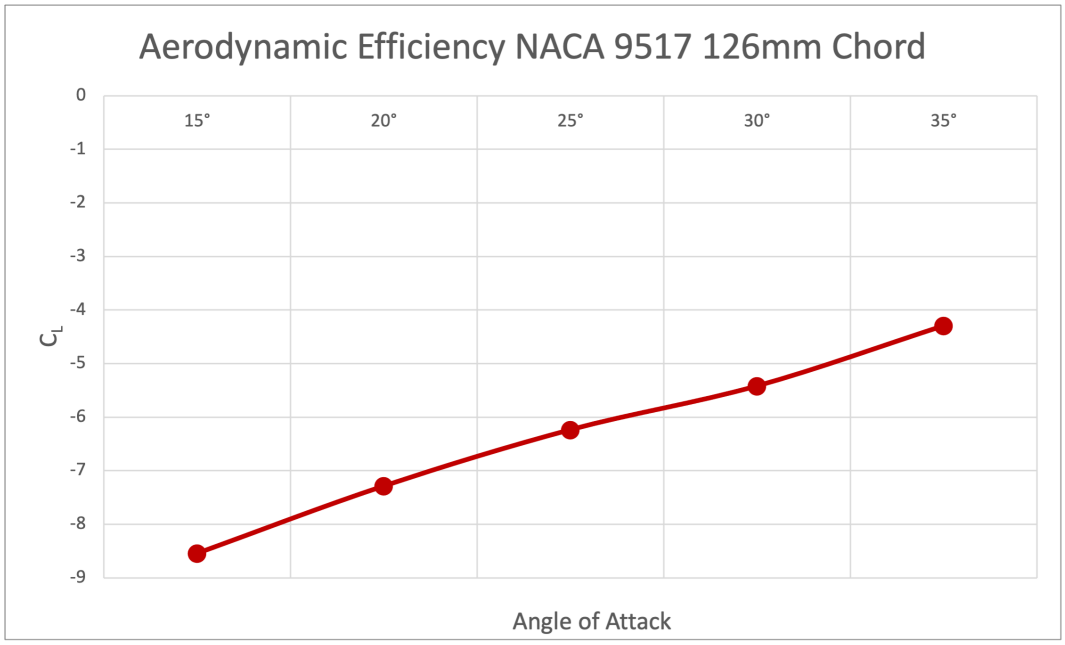

Figure 39: Representation of the aerodynamic efficiency with respect to the angle of attack of the E-423 airfoil with a chord of 324mm.

In this last analysis, it was also decided to increase the study range to 35 degrees, since at 30° the angle of loss had not been reached and angles with interesting efficiency could be found from this point onwards. Thus it was found that the angle of loss of this profile would be found infamously after 30 degrees.

As for the aerodynamic efficiency profile we found an almost linear evolution with a change of slope in the range between 25 and 30 degrees, which will be a case study when choosing a flap for the rear wing.

6.8 Conclusions

This section provides the CFD analysis of the 3 aerofoils as a whole, with the deepening of the most interesting angles. Their characteristics and efficiencies will be discussed and the most suitable ones will be chosen to compose the configurations to be analysed in the next section.

6.8.1 Selection of Aerofoils to Serve as Main Element

The results of the profiles with a 324 mm chord are discussed first. The findings are shown below:

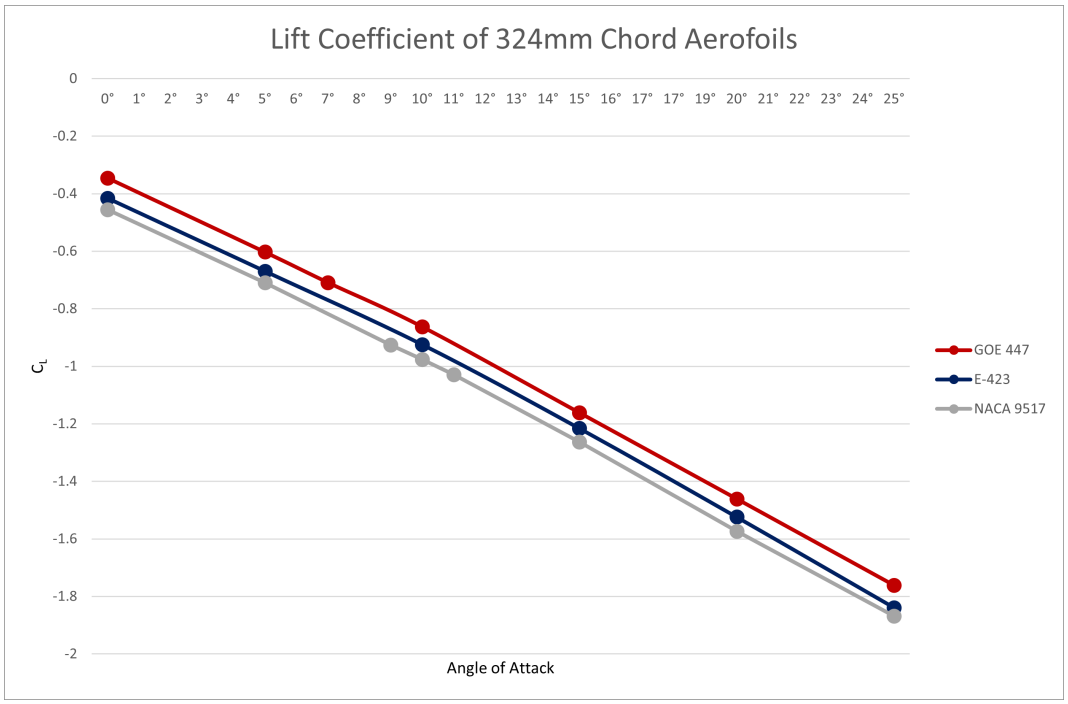

Figure 40: Representation of the lift coefficient versus angle of attack of the three airfoils chosen with a chord of 324mm.

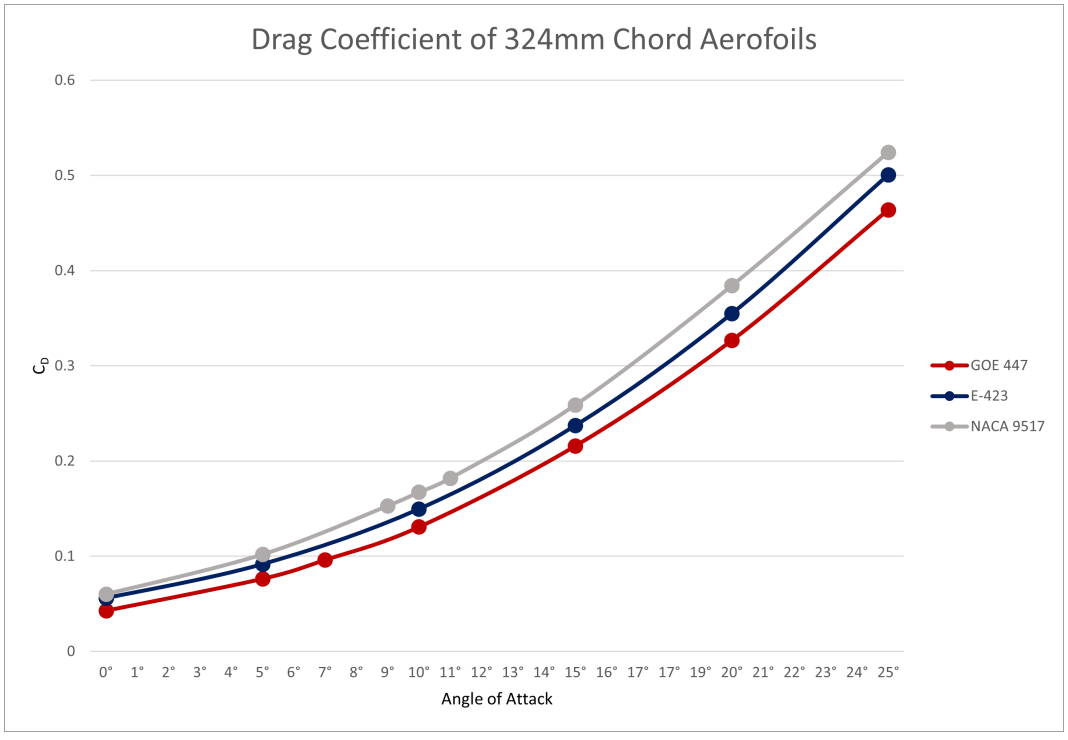

Figure 41: Representation of the drag coefficient versus angle of attack of the three airfoils chosen with a chord of 324mm.

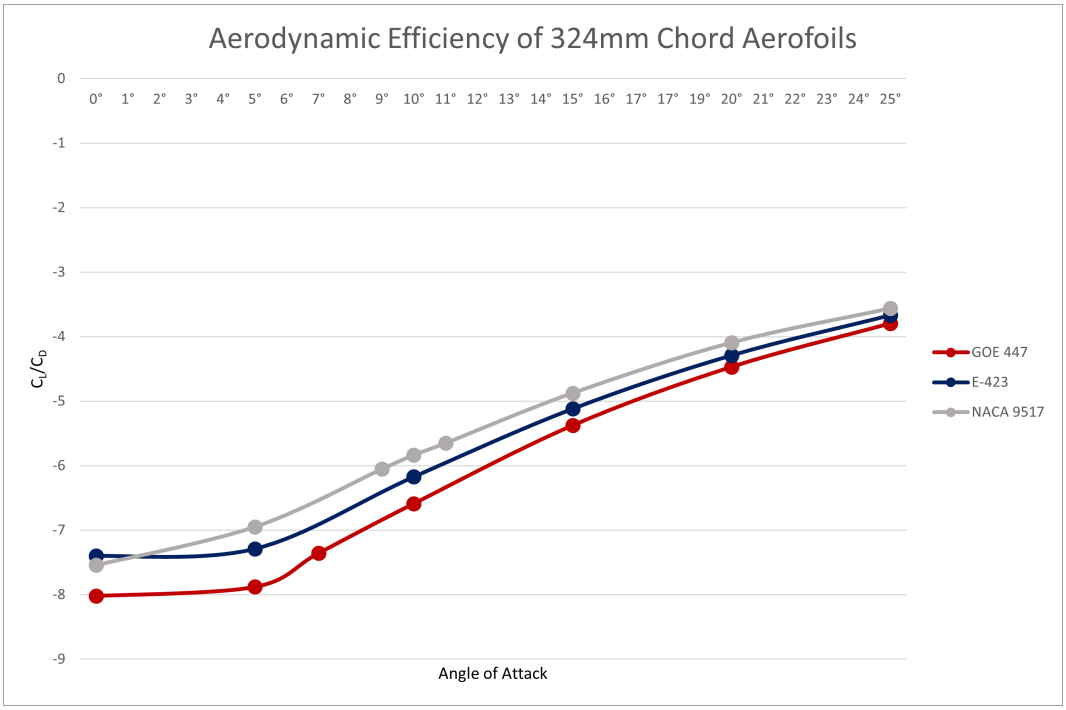

Figure 42: Representation of the aerodynamic efficiency coefficient versus angle of attack of the three airfoils chosen with a chord of 324mm.

As principal element of the aileron, the aim is to pursue the one that generates the least drag possible. Since the flap, having a greater angle of attack, will already generate a considerable amount of drag. The main element is thus intended to generate as minimal as possible of the total drag generated by the rear wing.

However, lift cannot be ignored. An airfoil that generates minimal drag must not be chosen if its lift coefficient is also minimal, as then the aerodynamic element would not be fulfilling its main function of generating downforce.

For this reason, on the one hand, the airfoil with the best aerodynamic coefficient is identified, which in this case is the GOE 447. In Figure 42, it can be noticed that for the whole range of angles of attack studied, the GOE 447 has a lower C_L/C_D than the remaining airfoils. However, such high angles are not of interest because this would imply an angle of attack too high for the flap and then it might stall.

Despite being the most aerodynamically efficient, the GOE 447 also yields the worst lift coefficient. However, a key point is the 5-degree angle of attack because, as mentioned above, although the anti-lift increases significantly, the drag does not rise as much. It was therefore examined whether the same tendency was repeated for larger angles (such as 7 degrees), i.e. whether the lift increased significantly in relation to the drag. The result,

as clearly seen in Figure 32, is negative: it is clear that for 7 degrees the lift increases as the drag does.

For the above reasons, the GOE 447 profile will be chosen as a possible principal element of the rear wing targeted by this project.

On the other hand, the performance of the airfoil that produces the best lift coefficient is analysed. This is because the generation of negative lift is the main function of these elements. It can be seen that in this case it is the NACA 9517 for the whole range of angles of attack studied. For this airfoil, compared to the others, its maximum efficiency position would be at 0 degrees. As its drag is low, close to that of the other two. However, the lift is still lower than that of the GOE 447 at 5 degrees, which has already been selected as a possible main airfoil.

Thus, the behaviour of the NACA 9517 at around 10 degrees is studied. It is in this zone, avoiding very high angles, that the C_L/C_D coefficient is closer to that of the other two profiles, while the anti-lift coefficient remains lower. The CFD studies carried out at 9 degrees and 11 degrees do not give any surprising results. The trend of the plotted curve is maintained.

Therefore, NACA 9517 with 324mm chord is also selected as a possible main airfoil. Thus it will be evaluated, in the next stage, whether it is worthwhile to prioritise lift over aerodynamic efficiency.

Aerofoil	**Angle of Attack**	$\boldsymbol{F_L}$	$\boldsymbol{F_D}$
GOE 447	5°	-20,0951777	2,550224147
NACA 9517	10°	-32,19402993	5,517175933

Table 11: Summary of the aerofoils chosen as possible main elements of the rear wing, their properties and results in the CFD study.

6.8.2 Selection of Aerofoils to Serve as Flap

The profiles designed for possible flaps are now analysed.

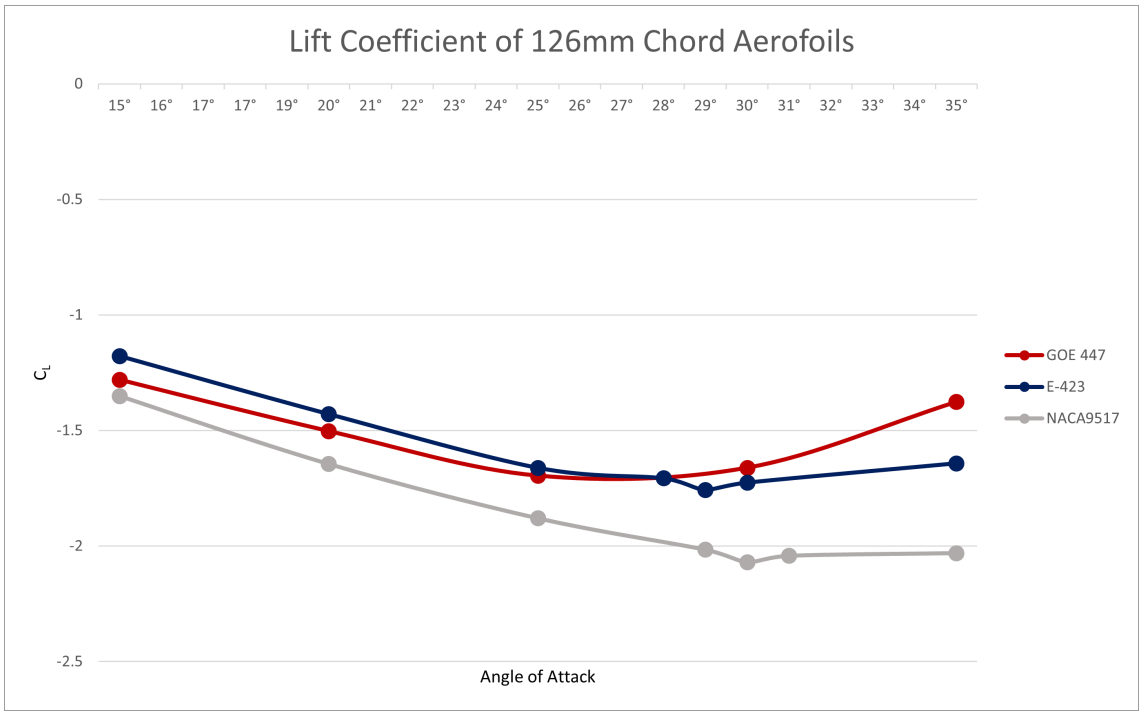

Figure 43: Representation of the lift coefficient versus angle of attack of the three airfoils chosen with a chord of 126mm.

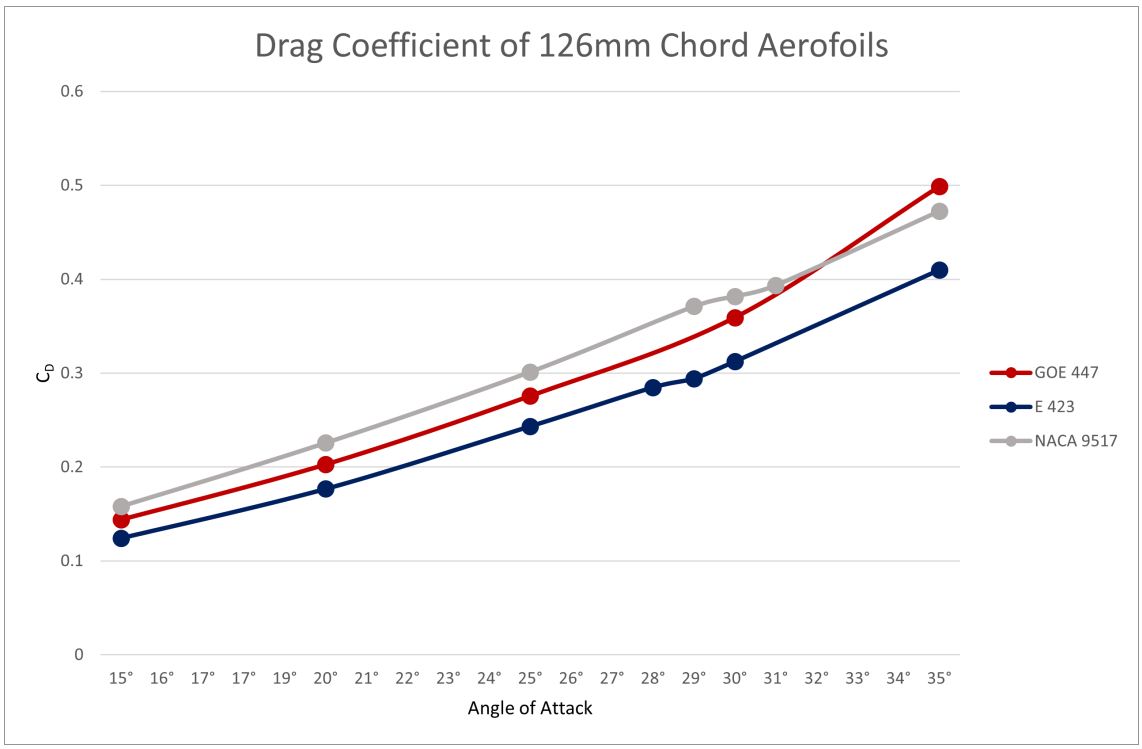

Figure 44: Representation of the drag coefficient versus angle of attack of the three airfoils chosen with a chord of 126mm.

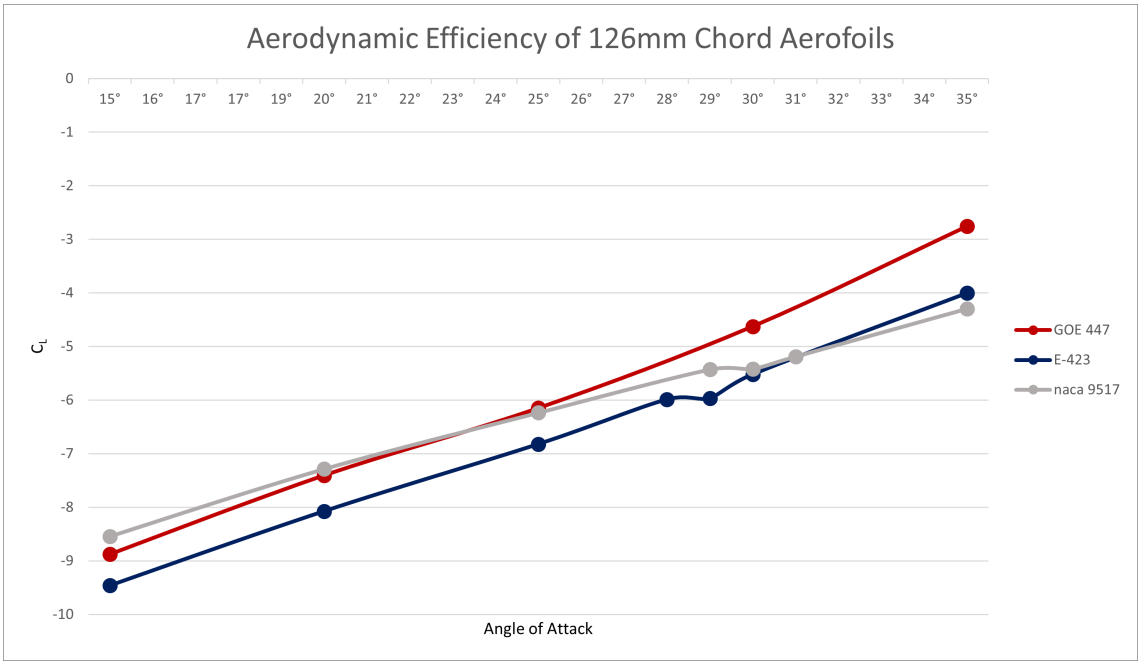

Figure 45: Representation of the aerodynamic efficiency coefficient versus angle of attack of the three airfoils chosen with a chord of 126mm.

The main consideration in the selection of the aileron's secondary element or flap is the amount of lift it will produce. Drag is not neglected. However, as mentioned in the previous section, all airfoils with a large angle of lift generate significant drag.

As for the stall angle of each airfoil, a first check showed that the GOE 447 was the first to reach this state. It was therefore discarded, as a single flap aileron requires a sufficiently high angle of attack from it.

Analyses were carried out at the points of interest to determine the exact stall angle of the other two airfoils. From these CDF calculations it was determined, as can be seen in Figure 43, that for the NACA 9517 airfoil the stall angle is reached at 30°. And for E-423 this angle is detected at 29°.

Focusing on Figure 43, it can be noticed that from 27 degrees onwards there is a notable difference between the downforce generated by the NACA 9517 airfoil and the E-423 one, being better for the the first one. Furthermore, looking at Figure 45, it can be seen that the aerodynamic efficiency of the NACA at around 29° is close to that of the E-423.

On the other hand, the E-423 airfoil, while having the best aerodynamic efficiency, has also the lowest anti-lift. This is not the intended purpose of the flap.

For the reasons mentioned above, the NACA 9517 airfoil at 29° will be selected as the flap for the rear wing to be designed in this Final Degree Project. Through this choice, without the risk of stall (if the maximum anti-lift angle of 30° is taken), a high downforce will be generated.

Aerofoil	**Angle of Attack**	$\boldsymbol{F_L(N)}$	$\boldsymbol{F_D(N)}$
NACA 9517	29°	-23,97997302	4,416330198

Table 12: Summary of the aerofoil chosen as flap of the rear wing, its properties and results in the CFD study.

7 Configurations Performance Analysis

This section shows and discusses the results of the CFD calculations of the different configurations. These are composed from the selection of profiles from the previous section. This will allow the configuration that best suits the objectives of this Final Degree Project to be chosen.

In these combinations, not only the aerofoils that compose them will vary, but also the chords of each one of them. As previously studied, for two-element ailerons the most efficient total chord distribution is usually between 25% and 30% of the total chord for the flap. Therefore, it will be tested which total chord allocation is most suitable for the purposes of this project.

The following table shows the different configurations that will be subjected to the CDF analysis:

Configuration Number	**Main Airfoil**	**Main's Chord**	**Flap Airfoil**	**Flap's Chord**
1.1	GOE 447	$75\%c = 337,5mm$	NACA 9517	$25\%c = 112,5mm$
1.2	GOE 447	$74\%c = 333mm$	NACA 9517	$26\%c = 117mm$
1.3	GOE 447	$73\%c = 328,5mm$	NACA 9517	$27\%c = 121,5mm$
1.4	GOE 447	$72\%c = 324mm$	NACA 9517	$28\%c = 126mm$
1.5	GOE 447	$71\%c = 319,5mm$	NACA 9517	$29\%c = 130,5mm$
1.6	GOE 447	$70\%c = 315mm$	NACA 9517	$30\%c = 135mm$
2.1	NACA 9517	$75\%c = 337,5mm$	NACA 9517	$25\%c = 112,5mm$
2.2	NACA 9517	$74\%c = 333mm$	NACA 9517	$26\%c = 117mm$
2.3	NACA 9517	$73\%c = 328,5mm$	NACA 9517	$27\%c = 121,5mm$
2.4	NACA 9517	$72\%c = 324mm$	NACA 9517	$28\%c = 126mm$
2.5	NACA 9517	$71\%c = 319,5mm$	NACA 9517	$29\%c = 130,5mm$
2.6	NACA 9517	$70\%c = 315mm$	NACA 9517	$30\%c = 135mm$

Table 13: Summary of the configurations formed from the selected aerofoils, with different chord values.

It should be noted that the angles of attack of the airfoils are those selected in the previous section (see Tables 10 and 11).

7.1 Endplates Design

One of the essential elements of the rear wings are the endplates. These plates are placed on the sides to prevent air from passing from the upper to the lower surface of the airfoils.

In order to approach one of the objectives of this Final Degree Project, that of reducing the cost of production, some plates recovered by the ApeCS team will be used to fulfil this function.

These plates were manufactured for the same purpose at an earlier time, therefore their design will be adjusted so that they can be used in an optimal way in the construction of the rear wing of the ApeCS single-seater.

Below is an image showing the initial dismensions of these plates:

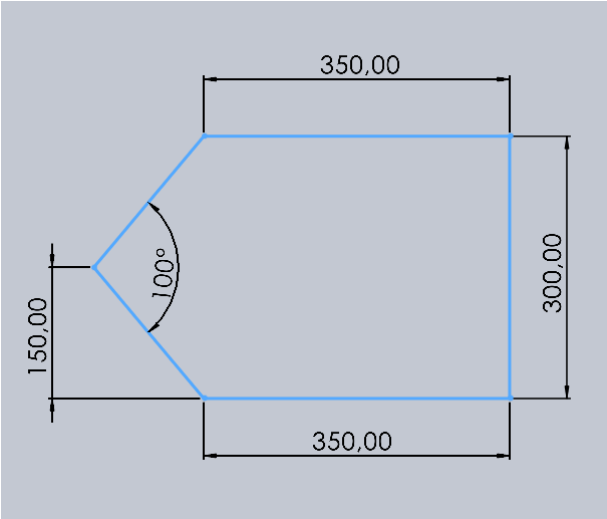

Figure 46: Sketch of the shape and dimensions of the initial endplates without rounded corners.

In order to improve the aerodynamics of these endplates, a horizontal section of the upper part of the endplate is removed to create a similar effect to that of the airfoils. A larger path at the bottom of the plate will increase the velocity of the air and this will lead to a decrease in pressure, thus generating a force oriented towards the ground.

Below is the final result of the dimensions of the rear wing endplates.

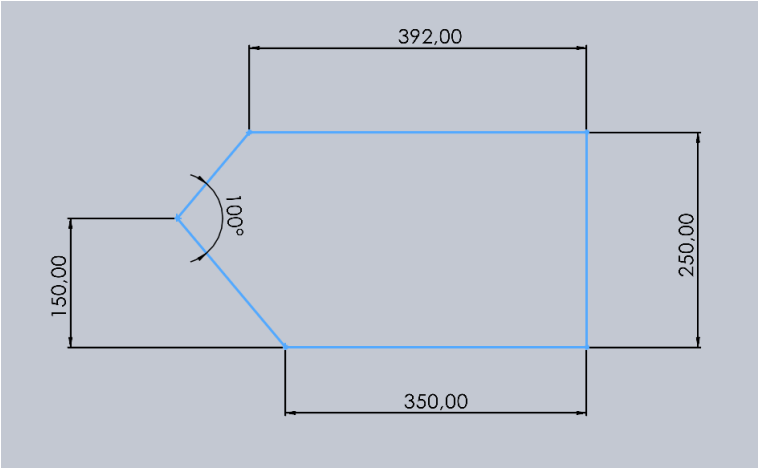

Figure 47: Sketch of the shape and dimensions of the final endplates without rounded corners.

The corners would simply need to be rounded to improve the security of the design.

7.2 Simulations, Analysis and Choice of Final Product

The following results have been obtained in the CFD analyses carried out for the simulations outlined in the previous section:

Configuration Number	$F_L(N)$	$F_D(N)$	F_L/F_D
1.1	-65,43	13,75	-4,76
1.2	-65,03	13,61	-4,78
1.3	-67,30	14,40	-4,67
1.4	-67,81	14,54	-4,66
1.5	-69,48	15,09	-4,60
1.6	-70,10	15,36	-4,56
2.1	-73,11	16,95	-4,31
2.2	-74,93	17,62	-4,25
2.3	-75,09	17,64	-4,26
2.4	-75,09	18,21	-4,12
2.5	-78,02	18,84	-4,14
2.6	-77,17	18,39	-4,20

Table 14: Results obtained from CFD calculations of different configurations for possible rear wing.

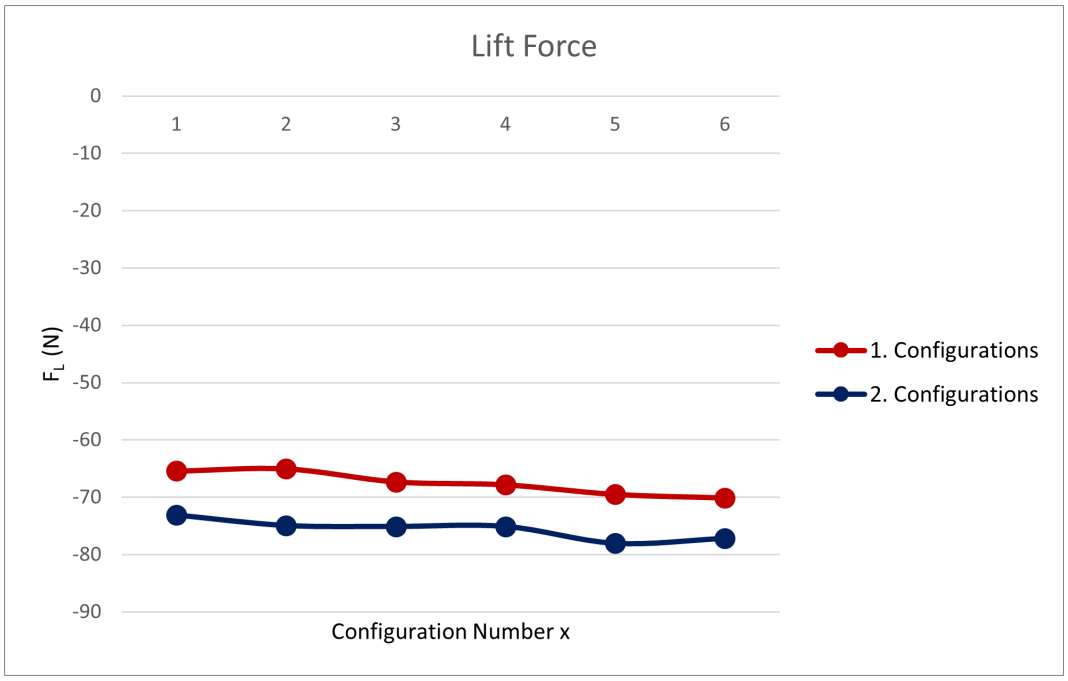

Figure 48: Representation of the lift force produced by the different configurations.

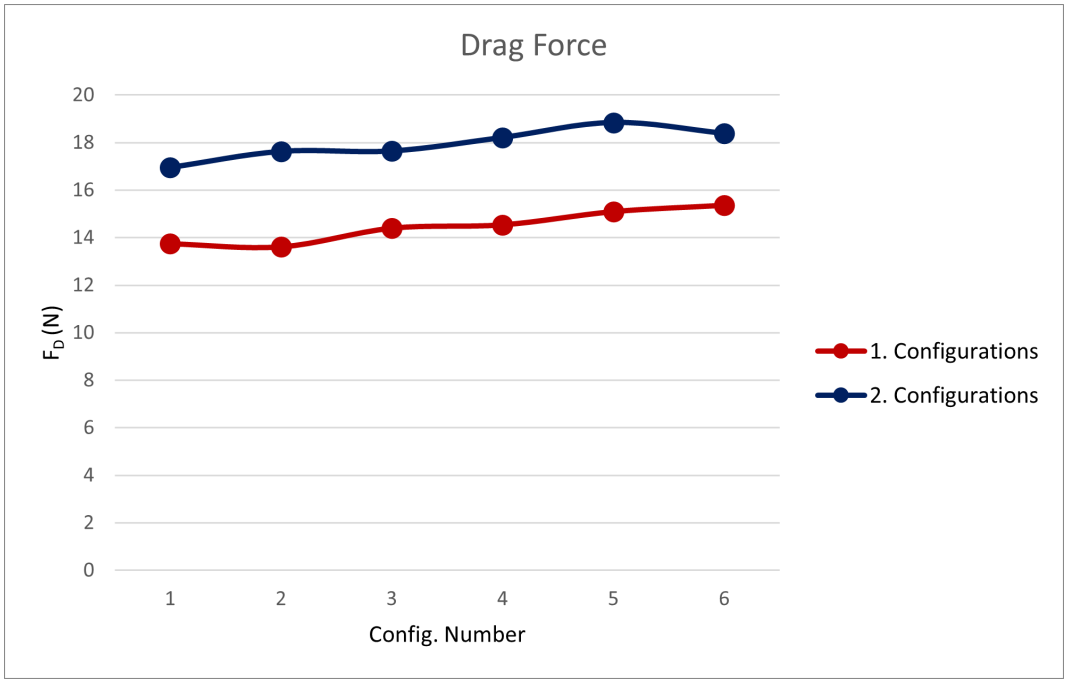

Figure 49: Representation of the drag force produced by the different configurations.

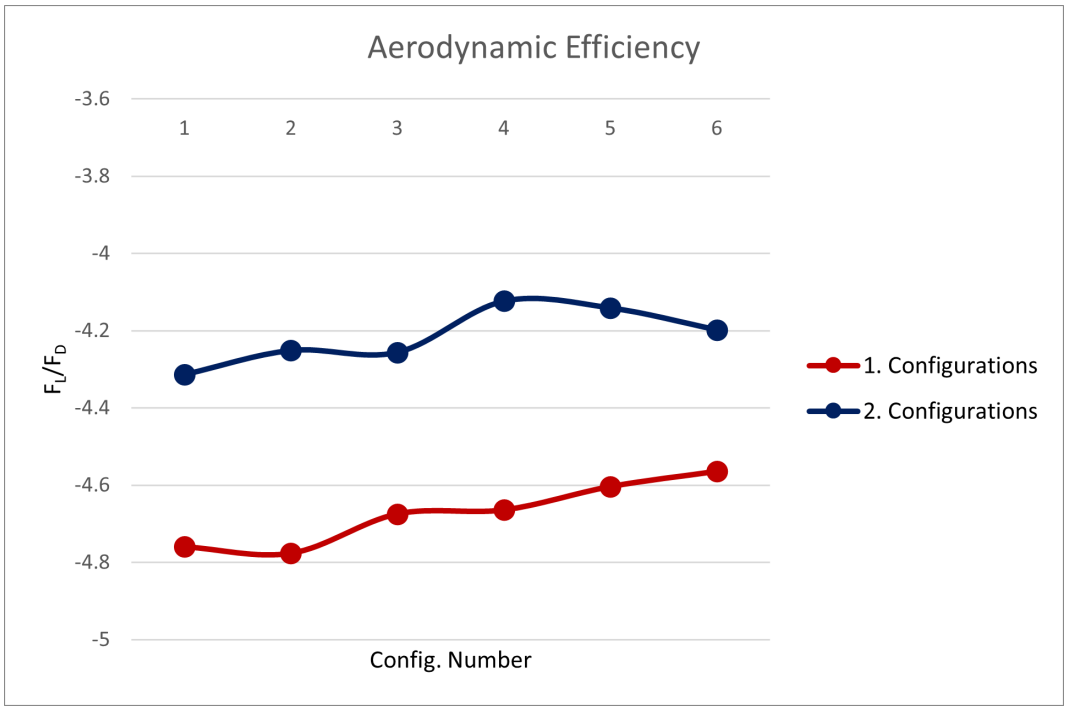

Figure 50: Representation of the aerodynamic efficiency of the different configurations.

Both Table 14 and Figures 48, 49 and 50 provide highly relevant information.

On the one hand, in the representation of the lift force, it is found that the configurations "2." always generate a greater anti-lift force. This was to be expected, as the main profile for these configurations (NACA 9517 at 10°) had a higher anti-lift coefficient than that of the "1." configurations (GOE 447 at 5°). In addition, it can be seen that as the size of the flap chord increases, the anti-lift also increases. This is due to the fact that it is the flap element of the wing that generates most of this force.

On the other hand, this difference in lift is also reflected in the drag focer graph. As expected, the configurations with the best lift are those with the highest drag. As occurs for the anti-lift force, and for the same reason, the drag increases as the flap size increases.

This results, as can be seen in Figure 50, in a better aerodynamic efficiency of the configurations "1." with GOE 447 as main airfoil at 5° angle of attack.

It is worth noting that, as can be seen in Tables 11, 12 and 14, the lift forces of the configurations do not correspond to the sum of the forces generated by the two separate airfoils. Thanks to the venturi effect, the small gap between the two profiles accelerates the flow. This results in a reduction of pressure and avoids the detachment of the boundary layer of the main airfoil.

Finally, since the difference in drag forces between the two types of configurations is not as significant as the difference in lift force, it is decided to choose a wing from the "2." configurations.

The 2.3 configuration is the one that provides the best results for the criteria of this project, offering the best ratio of lift and aerodynamic efficiency. Its drag is lower than that of other configurations (2.4) that give the same lift force result.

Therefore, the rear wing of the ApeCS Formula Student single seater will consist of a 328,5mm chord NACA 9517 airfoil with an angle of attack of 10° and a 121,5mm chord NACA 9517 airfoil flap with an angle of attack of 29°.

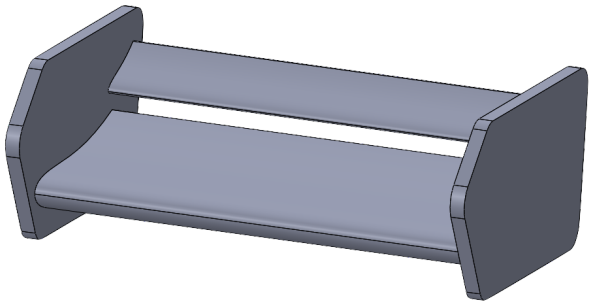

Figure 51: CAD desing of the 2.3 configuration.

7.3 Study of Performance and Potential Improvements to the Selected Wing

In this section an in-depth study of the final result of this Final Degree Project is provided, with the aim of analysing its potential with its strengths and possible weaknesses.

The distribution of total forces in the different components of the wing is shown below:

		Main Airfoil	Flap	Endplates	Total
Drag	**N**	9.60	6.54	1.51	17.64
	%	54%	37%	9%	
Lift	**N**	-61.11	-12.66	-1.31	-75.09
	%	81%	17%	2%	

Table 15: Distribution of forces generated by each element of the wing. Shown both in newtons and as a percentage.

From this table, the main airfoil's contribution to downforce is particularly noticeable. Around 80 percent of the downforce is generated by the main airfoil. However, it was apparent from Table 11 that the airfoil itself is not enough to produce these numbers. Other effects contribute to this result, such as the appearance of the flap, which causes the boundary layer of the main element to remain attached to it longer and therefore increases its produced downforce. The pressure and speed maps in the annex show that a zone of low speeds and high pressures is generated in the upper part of the wing, which is not as prominent with the isolated elements.

Furthermore, it should be noted that the flap generates less anti-lift force in the assembly than when tested alone. This difference is reflected in Figures 59 and 61 of Annex III. These velocity maps of the flap evaluated individually and in the configuration show the following: in the first one, it can be seen that there is a large difference in velocities on the leading edge between the upper and lower surfaces. This causes a great difference in pressures and a higher anti-lift force than that generated in the whole.Figure 59, which shows the velocity map of the configuration, reveals that there is also a difference, even across the entire flap surface. However, this variation is not noticeable enough to generate the same force as the flap on its own. One of the points to improve in this configuration would therefore be to increase the lift force of this flap in whole wing.

In addition, it can be seen from these results that the endplates also generate negative lift, which is expected as they were designed to do so. Nevertheless, this aerodynamic load could still be higher. A new design should be carried out for this sole purpose, but it is not within the scope of this project.

The analysis carried out in this section would be more accurate if it were performed on the entire vehicle. However, this has not been possible, as belonging to a newly emerging Formula Student team, the CAD design process of all the components of the vehicle has

not been completed.

An analysis of the aileron incorporated with the vehicle's whole body would probably give different results than those obtained, as some elements such as the main hoop of the chassis may interfere with the airflow incident on the wing.

8 Conclusions and Future Work

8.1 Conclusions

In the development of this project, the objectives set for the design of a rear wing for a Formula Student car have been achieved.

In terms of the objectives, this Final Degree Project has designed a spoiler that satisfies the restrictions required by the competition. In addition, throughout the study, the aim has been to ensure that the wing fulfils its main function, prioritising the generation of aerodynamic load but without neglecting resistance. As far as the design is concerned, we have tried to minimise the construction cost, reusing and reforming elements already manufactured or choosing airfoils with not very complex geometries.

It should be noted that while more advanced ailerons exist in other Formula Student teams, this is understandable due to the accumulated experience and the opportunity for iteration over the years. As far as this Final Degree Project is concerned, the designed wing represents a starting point and a fundamental step in the right direction.

8.2 Future Works

While this study provided valuable information on a first rear wing design and aerodynamic analysis for a Formula Student car, there are several opportunities for future research and improvements:

1. Comprehensive analysis of the car: One of the first steps to be taken after this project and once the complete car model is available will be to carry out a comprehensive CFD analysis that considers the interaction between all components.For this purpose, a previous design of the support that ensures the anchoring of the spoiler to the rest of the vehicle will be necessary. Once this analysis has been carried out, a more complete and accurate picture of the impact of the wing on the overall performance of the single-seater will be obtained.

2. Research into advanced materials: Another next step will be to investigate the use of advanced materials in the construction of the wing. The main objective would be to use lightweight technologies that improve the aerodynamic efficiency of the car,

such as carbon fibre. The choice of these materials will have to take into account the budget set by the team.

3. Design refinement: Finally, for future versions of the wing, it will be essential to consider adjustments to the airfoils and angles of attack. In this study, priority was given to downforce generation. However, future work could consider multi-objective optimisation, with more consideration given to factors such as drag minimisation.

ANNEXES

I Project Alignment with the Sustainable Development Goals (SDGs)

The motor racing industry is often not immediately recognised as a model of sustainable development due to its primary focus on optimising racing cars performance. However, competitions such as Formula 1 are already aiming for zero net carbon emissions by 2030. This Final Degree Project, centered around the design and analysis of a rear wing for a Formula Student competition car, might not inherently seem connected to sustainable development goals. However, a comprehensive examination reveals several ways in which this endeavor aligns with the United Nations Sustainable Development Goals (SDGs).

Directly tied to this project is *SDG 7 - Affordable and Clean Energy* , and more specifically *7.3 " By 2030, double the global rate of improvement in energy efficiency"*. The rear wing's objective includes minimizing drag, thereby enhancing energy efficiency and diminishing electricity consumption. Aerodynamics significantly influence a vehicle's energy consumption, making the design of an appropriate rear wing pivotal in curtailing this consumption. For instance, in major competitions, one of the programmes to achieve net zero carbon is "aeroactivity", which aims to actively modify the aerodynamics of vehicles during the race to reduce aerodynamic drag and, consequently, energy consumption.

Furthermore, the utilization of simulation technologies in this project contributes to *SDG 12 - Responsible Consumption and Production* . Software applications such as Ansys Fluid and SolidWorks eliminate the need to physically construct the rear wing for performance evaluation. This approach, grounded in modeling and simulation, substantially minimizes the environmental impact of rear wing innovations and fosters responsible resource consumption contributing to goal *12.2, achieve the sustainable management and efficient use of natural resources.*

Lastly, there is an indirect implication of this project on *SDG 9 - Industry, Innovation, and Infrastructure*. It is well known that advancements in motorsports often trickle down to the wider automotive industry. The incorporation of rear wing technology into standard automobiles could markedly enhance passenger safety during high-speed travel. Esteemed companies like Porsche, Bugatti, and Mercedes are already exploring rear wing innovations to maximize their efficiency, minimizing adverse effects at low speeds while augmenting benefits at high speeds.

In conclusion, this project's seemingly specialized focus on rear wing optimization for a Formula Student competition car remarkably aligns with a spectrum of UN Sustainable Development Goals. Through enhancing energy efficiency, embracing simulation technologies and inspiring broader industry innovation, this undertaking tangibly contributes to the pursuit of a more sustainable and equitable future.

II Pressure Contours

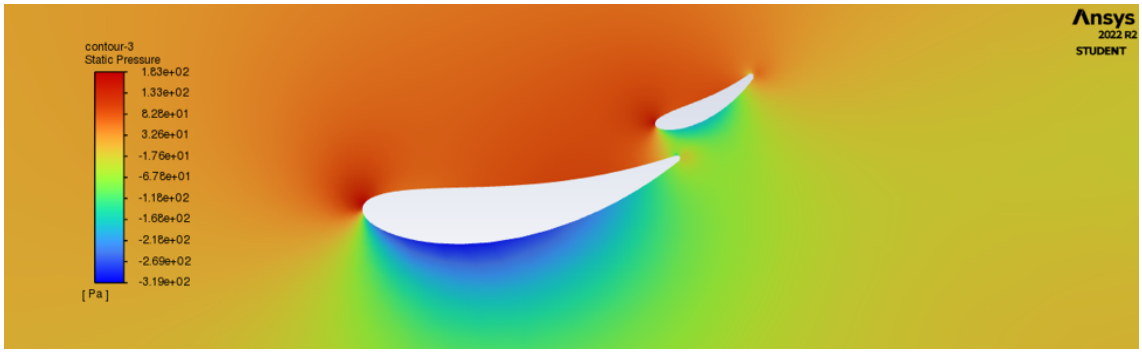

Figure 52: Pressure map in a plane parallel to the direction of flow which cuts the wing resulting from this Final Degree Project in half.

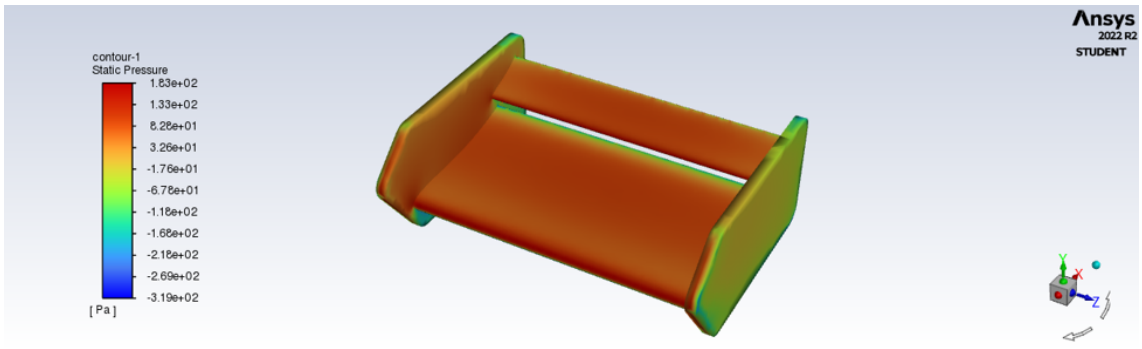

Figure 53: Contour of the wing, viewed from bellow, showing the pressures at each point on its surface.

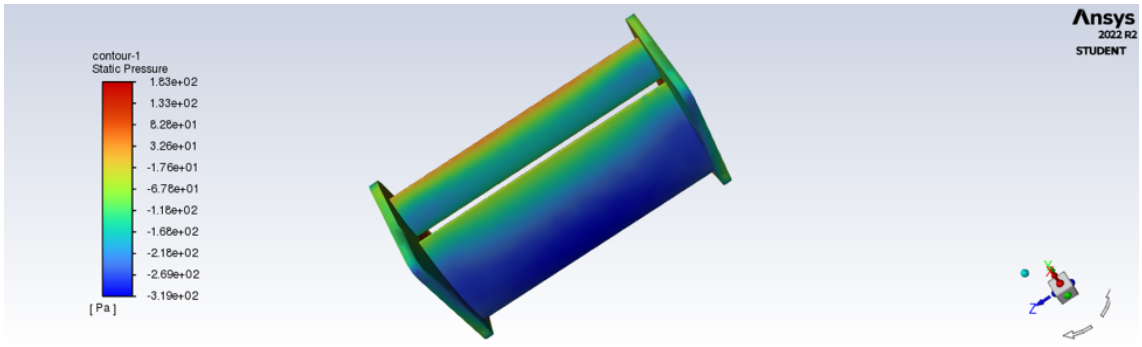

Figure 54: Contour of the wing, viewed from above, showing the pressures at each point on its surface.

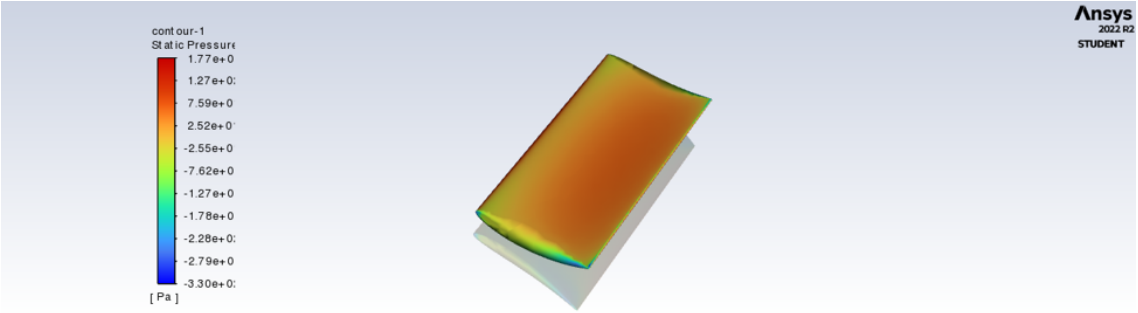

Figure 55: Top view of the NACA 9517 with 324mm chord and 10° angle of attack, which acts as the main element of the final wing. Representation of the pressures suffered at each point of its surface, when analysed individually.

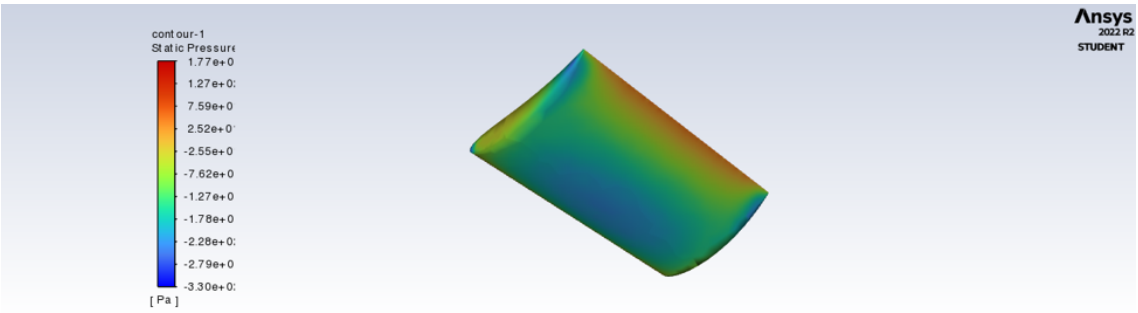

Figure 56: View from bellow of the NACA 9517 with 324mm chord and 10° angle of attack, which acts as the flap of the final wing. Representation of the pressures suffered at each point of its surface, when analysed individually.

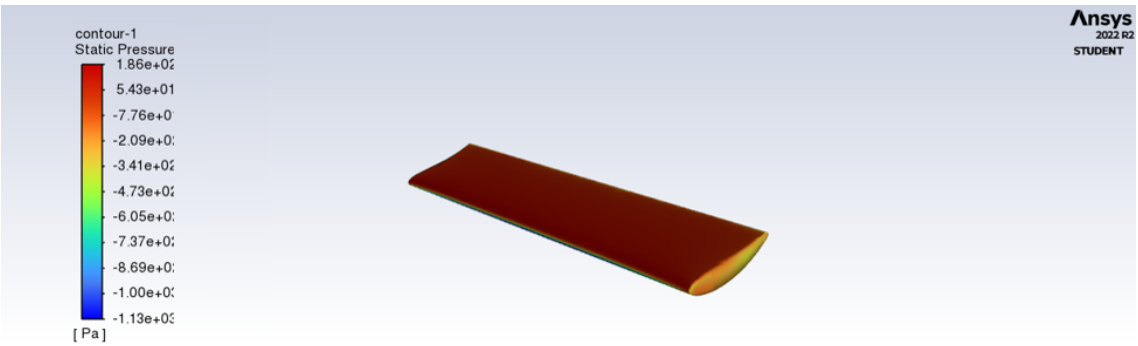

Figure 57: View from adove of the NACA 9517 with 126mm chord and 29° angle of attack, which acts as the flap of the final wing. Representation of the pressures suffered at each point of its surface, when analysed individually.

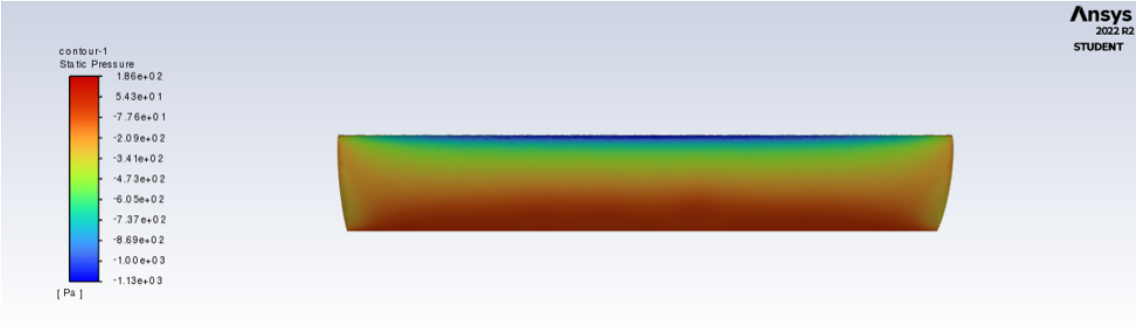

Figure 58: View from bellow of the NACA 9517 with 126mm chord and 29° angle of attack, which acts as the flap of the final wing. Representation of the pressures suffered at each point of its surface, when analysed individually.

III Speed Maps

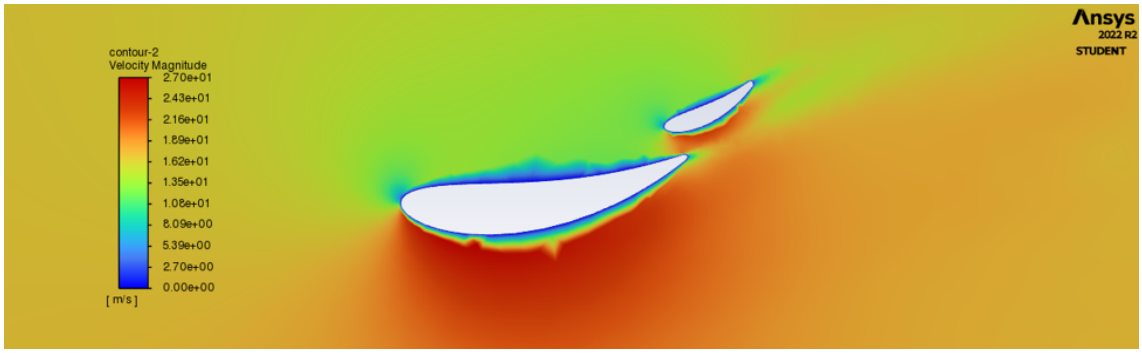

Figure 59: Speed map in a plane parallel to the direction of flow which cuts the wing resulting from this Final Degree Project in half.

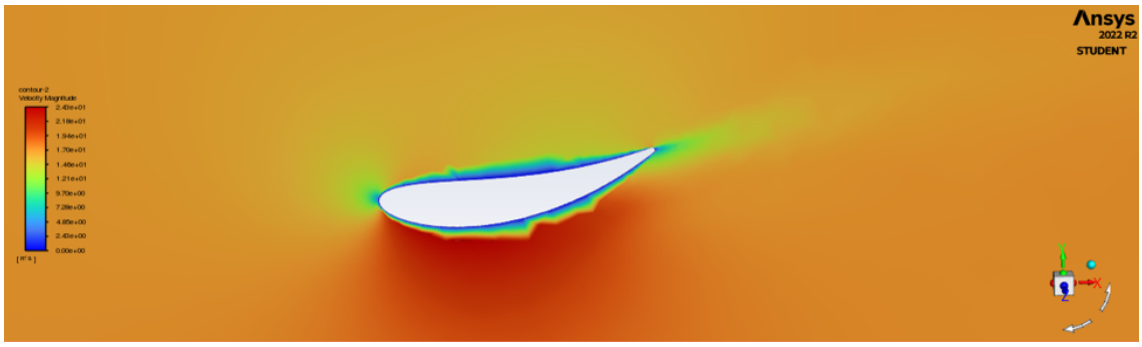

Figure 60: Speed map in a plane parallel to the direction of flow which cuts the NACA 9517 with a 324mm chord in half. Results of the individual analysis of this aerofoil.

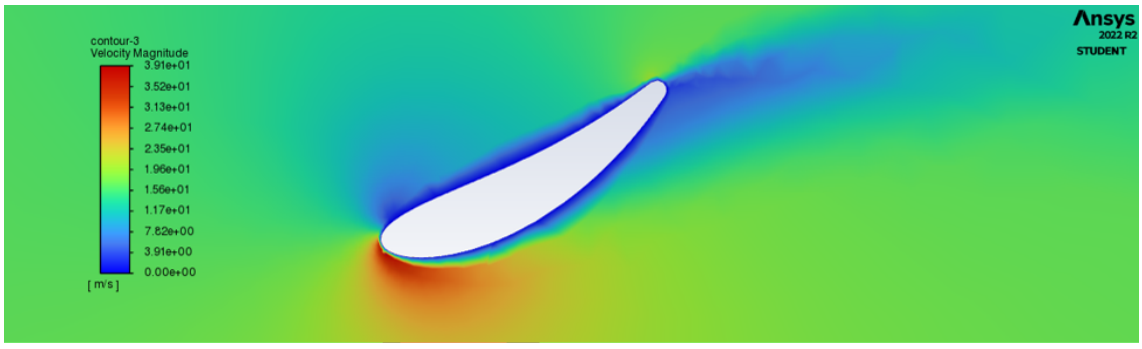

Figure 61: Speed map in a plane parallel to the direction of flow which cuts the NACA 9517 with a 126mm chord in half. Results of the individual analysis of this aerofoil.

BIBLIOGRAPHY

References

[Air] AirfoilTools.com. On-line: http://airfoiltools.com.

[Alt] AltairAcuSolve. Basic boundary layer theory. On-line: https://2021.help.altair.com/2021.2/hwsolvers/acusolve/topics/acusolve/training_manual/basic_boundary_layer_theory_r.htm.

[Bla22] Elisabeth Blackstock. This is the rumpler drop, the world's first streamlined car. On-line: https://jalopnik.com/this-is-the-rumpler-drop-the-worlds-first-streamlined-1848661136, 2022.

[dBC19] Circuit de Barcelona Catalunya. Empieza la décima edición de la formula student spain en el circuit. On-line: https://www.circuitcat.com/es/noticias/circuit/empieza-la-decima-edicion-de-la-formula-student-spain-en-el-circuit/, 2019.

[Dom23] Agustín Martín Domingo. Apuntes de mecánica de fluidos. 2023.

[ER22] University of Aerodynamics Embry Riddle. Introduction to aerospace flight vehicles. On-line: https://www.google.com/url?sa=iurl=https2022.

[F1] Aerodinámica F1. Historia de la aerodinámica en la f1. On-line: https://www.aerodinamicaf1.com/2019/09/historia-de-la-aerodinamica-en-la-f1/.

[F1T13] F1Technical. Why do leading edge of airfoils need to be rounded? On-line: https://www.f1technical.net/forum/viewtopic.php?t=14877, 2013.

[FSG22] FSG. Fsg competition handbook 2022. 2022.

[Gra] Graining. Cascada de flaps en alerones. On-line: https://www.grainingf1.com/cascada-de-flaps-en-alerones/.

[Lud70] Karl E Ludvigsen. The time tunnel-an historical survey of automotive aerodynamics. *SAE Transactions*, pages 99–113, 1970.

[McB15] McBeath. *Competition Car Aerodynamics*. 2015.

[Res] ResearchGate. On-line: https://www.researchgate.net/figure/Laminar-versus-turbulent-flow-Turbulent-flow-which-occurs-at-high-Reynolds-numbers_fig2_337810582.

[Rod17] Alberto Rodríguez. Análisis técnico – drs – drag reduction system. On-line: https://albrodpulf1.wordpress.com/2017/09/25/analisis-tecnico-drs-drag-reduction-system/, Sep 2017.

[Sie] Siemens. Formula student germany 2019 – the most advanced student competition in the world! On-line: https://blogs.sw.siemens.com/academic/formula-student-germany-the-most-advanced-student-competition-in-the-world/.

[Stu23] Formula Student. Formula student rules 2023. 2023.

[TIM21] THE CLASSIC TIMES.COM. Lotus type 49, una década dominando la fórmula 1 (1967-1968), 2021.

[Wika] Wikimediacommons. Fowler flap diagram. On-line: https://commons.wikimedia.org/wiki/File:Fowler_flap_diagram.svg.

[Wikb] Wikipedia. Chaparral cars. On-line: https://es.wikipedia.org/wiki/Chaparral_Cars.